



**HAL**  
open science

## Rheological behavior of stabilized diamond-graphene nanoplatelets hybrid nanosuspensions in mineral oil

S.U. Ilyas, S. Ridha, S. Sardar, Patrice Estellé, A. Kumar, R. Pendyala

### ► To cite this version:

S.U. Ilyas, S. Ridha, S. Sardar, Patrice Estellé, A. Kumar, et al.. Rheological behavior of stabilized diamond-graphene nanoplatelets hybrid nanosuspensions in mineral oil. *Journal of Molecular Liquids*, 2021, 328, pp.115509. 10.1016/j.molliq.2021.115509 . hal-03159331

**HAL Id: hal-03159331**

**<https://hal.science/hal-03159331>**

Submitted on 11 May 2021

**HAL** is a multi-disciplinary open access archive for the deposit and dissemination of scientific research documents, whether they are published or not. The documents may come from teaching and research institutions in France or abroad, or from public or private research centers.

L'archive ouverte pluridisciplinaire **HAL**, est destinée au dépôt et à la diffusion de documents scientifiques de niveau recherche, publiés ou non, émanant des établissements d'enseignement et de recherche français ou étrangers, des laboratoires publics ou privés.

# Rheological Behaviour of Stabilized Diamond-Graphene Nanoplatelets Hybrid Nanosuspensions in Mineral Oil

Suhaib Umer Ilyas<sup>a\*</sup>, Syahrir Ridha<sup>a,b</sup>, Suneela Sardar<sup>c</sup>, Patrice Estellé<sup>d</sup>, Abhishek Kumar<sup>b</sup>,  
Rajashekhar Pendyala<sup>e</sup>

<sup>a</sup>Institute of Hydrocarbon Recovery, Universiti Teknologi PETRONAS, 32610 Seri Iskandar, Perak Darul  
Ridzuan, Malaysia

<sup>b</sup>Petroleum Engineering Department, Universiti Teknologi PETRONAS, 32610 Seri Iskandar, Perak Darul  
Ridzuan, Malaysia

<sup>c</sup>School of Chemical and Process Engineering, University of Leeds, Leeds, LS2 9JT, United Kingdom

<sup>d</sup>Univ Rennes, LGCGM, 35000 Rennes, France

<sup>e</sup>Chemical Engineering Department, Universiti Teknologi PETRONAS, 32610 Seri Iskandar, Perak Darul  
Ridzuan, Malaysia

\*Corresponding Author: suhaib.ilyas@utp.edu.my

## Abstract

Recent advancements in thermo-fluid technology assisted with highly thermal conductive nanomaterials have shown assuring outcomes. It is also proven that thermal conductivity alone cannot define the overall heat transfer characteristics, and the viscous properties are equally significant towards thermal management. Therefore, this research involves investigating the rheological behavior of hybrid nanosuspensions containing high thermally conductive diamond and graphene nanoplatelets (1:1). These nanomaterials are dispersed in mineral oil using a two-step technique. Hybrid nanofluids' stability is achieved using a non-ionic stabilizer Span85, exhibiting no sedimentation for a minimum of five months. Nanomaterial characterizations are performed to study morphology, purity, and chemical analysis. The flow behavior of hybrid nanosuspensions is investigated at varying nanomaterial mass concentrations (0-2 %), temperatures (298.15-338.15 K), and shear rates (1-2000 s<sup>-1</sup>). Hybrid nanofluids exhibit shear-thinning behavior, which is also correlated with the Ostwald-de-Waele model. The temperature-viscosity relationship is well predicted using the Vogel-Fulcher-Tammann model. Hybrid nanofluids show a maximum enhancement of 35% viscosity at 2% concentration. A generalized two-variable correlation is used to express viscosity as a function of temperature and nanofluid concentration with an excellent agreement. Three different machine learning methods, i.e., Artificial Neural Network (ANN), Gradient Boosting Machine (GBM), and Random Forest (RF) algorithms are also introduced to predict the viscosity of hybrid nanofluids based on the three input parameters (temperature, concentration, and shear rate). The parity plots conclude that all algorithms can predict big-data viscous behavior with high precision.

**Keywords:** Diamond; Graphene Nanoplatelets; Hybrid Nanofluid; Machine Learning; Mineral Oil; Rheology.

## 1. Introduction

The continuous increase in global energy demand and consumption has motivated researchers towards thermal management and energy optimization. Nanofluids can play a key role in thermal management due to superior thermal properties. The research on nanofluid technology is tremendously progressed

44 in recent years. The introduction of nanomaterials in conventional fluids, termed as nanofluids, modifies  
45 positively the physical, optical, electrical, and magnetic properties of the fluid [1,2]. The initial research  
46 on nanofluids two decades ago was primarily focused on increasing the thermal conductivity of fluids  
47 by adding metallic, non-metallic, carbon-based, and polymeric nanoparticles. Whereas, fewer  
48 contributions were observed towards flow characteristics and other temperature-dependent properties  
49 of nanosuspensions. The advancements in nanofluid research have proclaimed that the overall heat  
50 transfer performance of fluid may not depend solely on the thermal conductive parameter. Still, the  
51 effective viscosity, density, heat capacity, thermal expansion coefficient, and surface tension are equally  
52 important. The understanding and consideration of momentum transport during nanofluid operation in  
53 different applications is vital in achieving proficient thermal management of energy devices. A recent  
54 report [3] has stated several challenges in nanofluid technology towards industrial applications, such as  
55 low stability, increased pumping power for forced convective applications, reliability of conventional  
56 models, correlations, and reported experimental data.

57 Highly Refined Mineral Oils (HRMO) are generally used in several heat transfer applications where  
58 high-flux conditions or electrically insulating conditions are required, such as distributor transformer  
59 cooling, reactor cooling jackets, sub-merged cooling of electronic devices, automobile engine  
60 management, etc. [4,5]. Oil-based nanofluids are still not a well-developed research area but recently  
61 reported studies [6] had explored its potential in several applications. These applications of HRMO are  
62 not limited to heat transfer only, but it is also used in Enhanced Oil Recovery (EOR), cosmetics, food,  
63 lubrication, solar, and biomedical applications [7–10]. Asadi et al. [5] stated in a review study that  
64 nanofluids (oil-based) generally have a higher viscosity than the conventional liquids, which can  
65 increase the pumping power. Therefore, it might not be favorable for the heat transfer operation. The  
66 viscous properties are influenced by nanomaterial type, size, loadings, shear rate, and temperature.  
67 Therefore, it is essential to understand the flow behavior of nanofluids. Reported studies have  
68 mentioned the potential of HRMO with nano-additives as an excellent lubricating agent with anti-wear,  
69 reduced friction, tribological potential, and with the characteristics of improved load carrying capacity  
70 [11,12].

71 Several experimental studies have been published on the thermal and viscous transport properties of  
72 hybrid nanofluids in recent years. From a practical point of view, it is also possible that the flow  
73 behavior of nanofluids may exhibit Newtonian or non-Newtonian flow characteristics depending on the  
74 nanoparticle type, dimensions, and concentrations [13]. Zyla et al. [14] experimentally measured the  
75 rheological behavior of nano-diamond dispersions in ethylene glycol-based nanofluids. The nanofluids  
76 showed non-Newtonian behavior, referring to Herschel-Bulkley fluids. It was also observed that the  
77 viscosity of nanofluids increased with the diamond fraction. In an investigation on rheological studies  
78 of carbon black/ethylene glycol nanofluids by Zyla [15], it was found that the lowest concentration  
79 (0.001%) showed the Newtonian character. However, all other nanofluid concentrations exhibited non-  
80 Newtonian shear thinning behavior. Heris et al. [16] experimentally investigated rheological  
81 characteristics of ZnO-based nano-lubricants with varying concentrations from 0.1% to 4%. It was  
82 observed that nanofluids exhibited non-Newtonian Bingham fluid behavior.

83 Several reported studies [17,18] have suggested that hybrid nanofluids in the fluids could exhibit  
84 enhanced characteristics. Hybrid nanofluids are termed when more than one nanomaterials are added  
85 into the conventional liquid [9,19]. It is notable to mention that almost all studies referring to hybrid  
86 nanofluids have mechanically mixed nanomaterial combinations in different proportions to the base  
87 liquid, and there are no chemical interactions/bonding involved among the nanomaterials prior to  
88 mixing. Babu et al. [20] stated that hybrid nanofluids have a synergistic effect that could improve  
89 rheological characteristics and efficient thermal network. Asadi et al. [21] investigated experimental

90 dynamic viscosity of hybrid aqueous nanofluid containing CuO and TiO<sub>2</sub> nanoparticles. All nanofluids  
91 exhibited Newtonian character, and the highest concentration (1 vol%) showed the highest viscosity,  
92 1.74 mPa·s. Yan et al. [22] measured the dynamic viscosity of a hybrid nanofluid containing MgO and  
93 MWCNT dispersions in ethylene glycol. All nanofluids exhibited Newtonian character, and a maximum  
94 increase of 168% was reported for 1 vol% concentration. Afrand et al. [23] used SiO<sub>2</sub> and MWCNT  
95 hybrid dispersion in SAE40 oil to investigate viscous flow behavior at varying temperatures (298.15-  
96 323.15K) and concentrations (0–1 vol.%). The viscosity increased by a maximum of 37.4% and showed  
97 Newtonian behavior. Giwa et al. [24] studied the viscosity of water-based hybrid nanofluids containing  
98  $\gamma$ -Al<sub>2</sub>O<sub>3</sub> and MWCNT. They reported a maximum enhancement of 26.3% in viscosity at 328K using a  
99 90:10 ratio of the nanomaterials mentioned above. Tian et al. [25] investigated rheological parameters  
100 for CuO-MWCNT dispersions in water/EG (70:30) and reported that the highest nanomaterial  
101 concentration exhibited non-Newtonian characteristics. Alarifi et al. [26] experimentally investigated  
102 the rheological behavior of TiO<sub>2</sub>-MWCNT hybrid dispersions in oil. The nanofluids were found stable  
103 for 14 days, and the maximum enhancement (42%) was observed at 2% concentration and 50°C.

104 The progression in modeling the nanofluids' viscosity has suggested that the conventional models may  
105 not accurately predict nanofluids' thermophysical properties [3,5,27]. These conventional models do  
106 not consider agglomeration effect, sorption, double electrical layers, temperature, Brownian motion,  
107 etc. in their equations. Thus, underpredicting the effective viscosity of nanofluids, which is observed in  
108 many studies [23,28,29]. Banisharif et al. [30] reported that a good agreement with the existing models  
109 could be achieved in the nanofluids' thermal conductivity by considering the nanolayer effect, effective  
110 medium theory, and Brownian motion. Asadi et al. [5] reviewed and compiled a list of correlations  
111 based on experimental data to predict oil-based nanofluids' effective viscosity. These correlations have  
112 no physical justifications and are valid for a specific type and range of nanofluids, depending on the  
113 trend of experimental data. The reported literature has proposed alternative prediction approaches using  
114 machine learning algorithms. Some of the commonly used machine learning techniques in nanofluid  
115 thermophysical properties predictions are Artificial Neural Network (ANN), Genetic algorithm (GA),  
116 Particle swarm optimization (PSO), radial basis function (RBF), and Least-square support vector  
117 machine (LSSVM), Random Forest (RF), Gradient Boost Method (GBM), etc. [31–33]. Dalkilic et al.  
118 [34] compared ANN predictions with the existing correlations for graphite/water nanofluid's dynamic  
119 viscosity. It was reported that the ANN method was better than correlation development. Gholizadeh et  
120 al. [35] used RF approach to predict the viscosity of metallic oxides-based nanofluids and reported  
121 0.989 R<sup>2</sup> for the model accuracy using multi-input parameters. It is noteworthy to mention that while  
122 the results obtained by machine learning predictive methods proliferate, the inner working of these tools  
123 remains elusive when it comes to physical insights or scientific principles. The flow of network  
124 processes information to solve a problem is often unclear. These predictive methods only depend on  
125 the number of data points, algorithm and trend of data provided.

126 Carbon-based nanomaterials generally possess high thermal conductivity [36], and several research  
127 groups are focusing on diamond and graphene nanomaterials to fully understand their potential in  
128 different applications. Diamond nanoparticles possess interesting mechanical, optical, thermal, and  
129 electrochemical properties. The high thermal conductivity of diamond nanoparticles makes it an ideal  
130 candidate for nanofluids-based thermal systems. It has a thermal conductivity of 2200-3320 W/m·K  
131 due to low photon scattering and strong carbon covalent bonding [37]. Besides high thermal  
132 conductivity, it has negligible electrical conductivity (~0.01 nS/m), which may have great potential for  
133 electronic cooling systems. Graphene nanomaterials are competitive with unique thermal, mechanical,  
134 optical, and electrical properties [38]. It has a 2D structure with strong covalent bindings in the form of

135 a hexagonal carbon network. It has proven to be a significant agent for high-frequency nanoelectronics,  
136 supercapacitors, chemical sensors, EOR, etc. [39–41].

137 This research aims to investigate the rheological behavior of hybrid nanofluid with different  
138 concentrations of diamond nanoparticles and graphene nanoplatelets dispersions in HRMO. Both  
139 nanomaterials are among the highest thermal conductive materials. It is believed that this combination  
140 in HRMOs-based nanofluids may provide and explore a new class of advanced nanofluid for thermal  
141 management issues. Therefore, these nanofluids' flow behaviour is experimentally studied in this  
142 research at varying mass concentrations, shear rates, and temperature. It is also notable that such a  
143 combination of hybrid nanofluid has not been subjected to research before. Thus, exhibiting the novelty  
144 of this research. Initial nanomaterial characterizations are performed to study morphology, topology,  
145 crystalline nature, and chemical purity composition. The hybrid nanofluids are then prepared using a  
146 non-ionic surfactant, and stability is evaluated for over five months. A rotational rheometer is used to  
147 analyze the viscosity of hybrid nanofluids experimentally. Different models and correlations are applied  
148 to express and characterize the nature of rheology experiments. Three machine learning approaches  
149 have also been utilized to predict complete experimental data of viscosity of hybrid nanofluids.

## 150 **2. Methodology**

### 151 **2.1 Materials**

152 A combination of two nanomaterials is used in this research, i.e., diamond nanoparticles and graphene  
153 nanoplatelets. Diamond nanoparticles are acquired from US Research Nanomaterials, Inc. (USA),  
154 having nearly spherical morphology with an average diameter size of 3-10 nm and specific surface area  
155 (SSA) of 272 m<sup>2</sup>/g. The true density of diamond nanoparticles is 3.05-3.30 g/cm<sup>3</sup> with a purity of  
156 >98.3%. Graphene nanoplatelets are acquired from Sigma-Aldrich Malaysia with 750m<sup>2</sup>/g SSA. The  
157 average size of the nanoplatelet is <2 μm, and an average thickness of 10 nm. The molecular weight of  
158 nanoplatelets is 12.01, and the true density is 2.25 g/cm<sup>3</sup>. A hybrid nanomaterial system is created by  
159 adding diamond nanoparticles and graphene nanoplatelets in an equal mass ratio (1:1) in the base fluid.  
160 Both nanomaterials are not chemically bonded and dispersed in the oil without any alteration; thus, the  
161 structure and dimensions of nanomaterials are not affected.

162 The base fluid is highly refined mineral oil (HRMO), Caltex Texatherm 32, consisting of 70-99 wt%  
163 hydrocarbons (C15-C50). Non-ionic sorbitane trioleate (Span 85) is used as a stabilizing agent acquired  
164 from Sigma-Aldrich, Malaysia. These specifications of nanomaterials and the base-fluid are provided  
165 by manufacturing companies, and investigations are performed without altering any chemical or  
166 mechanical nature of the materials. However, characterizations are performed in this research to verify  
167 the morphology and purity of nanoparticles.

### 168 **2.2 Nanoparticle Characterization**

169 Different characterization techniques are used to confirm the structure, morphology, and elemental  
170 composition of nanomaterials and diamond and graphene nanoplatelets hybrid mixtures. In this  
171 research, Field Emissions Scanning Electron Microscopy (FESEM), (Zeiss-Supra 55VP, Germany), is  
172 employed to study the morphological feature of diamond and graphene nanoplatelets. Samples for  
173 FESEM analysis are prepared by dispersing the nanomaterials in the acetone and ultrasonically vibrated  
174 for several minutes. A droplet from the obtained suspension is transferred to the clean aluminium stub  
175 and dried for a few minutes. Nanomaterials are inspected for morphological characterization using  
176 Transmission Electron Microscopy (TEM), (Hitachi HT7830UHR, Japan), for crystallinity.

177 Nanoparticles were dispersed in acetone by sonication and drops of formed suspensions were  
178 introduced onto holey carbon-coated copper grids for analysis. Energy Dispersive X-ray (EDX)  
179 spectroscopy is used for the estimation of elemental composition. Structural characterization of  
180 nanomaterials is performed using powder X-ray Diffraction (XRD), (Bruker D8, USA), employing  
181  $\text{CuK}\alpha$  radiation ( $\lambda = 1.5418 \text{ \AA}$ ) at ambient conditions. For XRD, scans are performed over a  $2\theta$  ranges  
182 from  $20\text{-}70^\circ$  with a step size of  $0.1^\circ$ . In addition to structural and morphological features, Fourier  
183 Transform Infrared Reflection spectroscopy (FTIR) is used to determine the qualitative features of IR-  
184 active molecules in nanomaterials. It can also provide information about the light elements such as H  
185 and C in inorganic substances. In this research, the experiment is carried out by FTIR (Perkin Elmer,  
186 USA) with a diamond iTR attenuated total reflectance (ATR) sampling accessory. The spectra are taken  
187 over the wavenumber ranging  $400\text{-}4000 \text{ cm}^{-1}$  and 36 scans are used per spectrum.

### 188 **2.3 Preparation and Stability of Nanofluids**

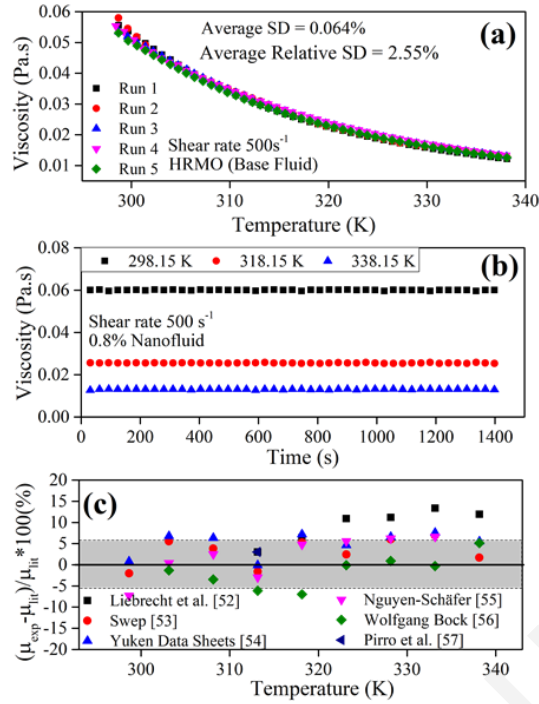
189 The hybrid nanofluids are prepared by mechanically mixing diamond nanoparticles and graphene  
190 nanoplatelets in equal mass proportions (1:1) and dispersing into HRMO using the two-step method.  
191 Generally, the solid nanomaterials are prone to settle down due to aggregation among particles [42,43].  
192 This aggregation is subjected to surface interaction of nanomaterials, where Van der Waal attractive  
193 forces are the strongest. Hence, increasing the primary size of the nanomaterials to a micron-level and  
194 settling down due to gravity. A destabilized nanofluid is considered not valid for any practical  
195 application. Therefore, it is essential to evaluate the stability of nanofluids prior to any thermophysical  
196 property measurement. In this research, the ultrasonication method and a non-ionic surfactant are  
197 utilized to stabilize hybrid nanomaterials in HRMO for a longer time. An ultrasonic homogenizer  
198 (probe), (Biologics 150V/T, USA), is used with frequency 20 kHz. The optimized ultrasonic parameters  
199 are taken from previous studies [41,44,45], i.e., 1 hr operation, 30% pulse and 70% power. This  
200 indicates that each nanofluid sample is ultrasonicated with a 70% power of the equipment's total  
201 ultrasonic frequency. The pulse indicates the cycle time (on/off), which is set at 30% for safer operation  
202 of the equipment. A water bath is used to avoid heating the hybrid nanofluid sample during ultrasonic  
203 operation. A non-ionic surfactant, Span 85, is used to stabilize hybrid nanoparticles in HRMO. The  
204 basis of choosing non-ionic surfactant in this research is that it does not aid in corrosion during  
205 operation. It has high thermal stability, non-toxicity, environment-friendly, non-foaming quality during  
206 operation, and highly compatible with HRMO. Generally, non-ionic stabilizers have no charge at the  
207 hydrophilic end, and the linkage of particles and base fluid relies on steric hindrance only [46].  
208 Therefore, a higher quantity of non-ionic surfactant may be required compared to ionic surfactants to  
209 achieve better nano-dispersion. In this research, hybrid nanofluids are prepared at six different mass  
210 concentrations i.e., 0, 0.4%, 0.8%, 1.2%, 1.6% and 2%. Few experiments are conducted to find the  
211 optimum concentration of surfactant required to stabilize nanofluid. The optimum mass concentration  
212 of hybrid nanomaterial to surfactant (Span85) ratio is found to be 1:5. The evaluation of stability is  
213 performed by visual inspection. Several studies have performed zeta potential analysis and UV-Vis UV-  
214 Vis Spectroscopy to evaluate stability. However, these analyses are not included in this research. Zeta  
215 potential is highly dependent on the pH of the nanofluid system. This research involves mineral oil as  
216 a base fluid which does not have pH; hence, zeta potential analysis might not give results precisely.  
217 Furthermore, the concentrations of hybrid nanofluids are relatively high than dilute fluid. The UV-Vis  
218 light beam is unable to pass through the dense sample concentration; hence, unable to detect any  
219 measurement. Therefore, only visual analysis is performed to investigate the stability of nanofluids. The  
220 experiments to characterize rheology is performed for the fresh samples of hybrid nanofluids containing  
221 stabilizer. The addition of surfactant may change the overall viscosity of nanofluid [47,48]. Therefore,

222 a comparative experimental investigation is also performed (Section 3.3.3) to evaluate the impact of  
223 surfactant on the effective viscosity.

## 224 **2.4 Rheology Experiments and Validation**

225 The rheological behavior of diamond-graphene nanoplatelets-based hybrid nanofluids is experimentally  
226 measured by the DHR1 rheometer by TA Instruments (USA) under steady shear flow conditions. The  
227 temperature is kept constant for each shear ramp conditions set at 10 data points per decade from shear  
228 rate 1 to 2000 s<sup>-1</sup>. The shear ramp conditions are used at five different temperatures for all samples, i.e.  
229 298.15K, 308.15K, 318.15K, 328.15K, and 338.15K. The geometry of the rheometer is steel-made cone  
230 and plate with a 2° cone angle, 55 μm truncation gap, and 60 mm diameter. The temperature of the  
231 system is controlled by a Peltier-plate system with 0.05 K accuracy. The readings are measured at a  
232 constant shear rate/time step. Initially, a constant volume of sample is carefully introduced in the testing  
233 cell rested for a few minutes before the operation to avoid bubble formation. Fresh samples are utilized  
234 for repeatability and each shear ramp at different temperatures. The test cell is carefully cleaned by  
235 solvents after each shear ramp test.

236 The uncertainty in the measurements is evaluated by following the methodology adopted in the  
237 literature [49–51]. Figure 1(a) presents the repeatability data for HRMO at temperature-ramp conditions  
238 from 298.15K to 338.15K. The viscosity is measured for five fresh samples of HRMO at a constant  
239 shear rate of 500 s<sup>-1</sup>. The repeatability of the sample shows an average standard deviation (SD) of  
240 0.064% and average relative SD of 2.55%. The 0.8% nanofluid sample is tested at three different  
241 temperatures (i.e., 298.15K, 318.15K, and 338.15K) and a constant shear rate of 500 s<sup>-1</sup> to check the  
242 thermal stability and accuracy of the measurements, shown in Figure 1(b). The readings are taken every  
243 31 seconds for a total of 1400 seconds. It is observed that the nanofluid is capable of withstanding high  
244 temperature, and the slight deviations in viscosity readings are almost negligible. Figure 1(b) also  
245 proves that effective viscosity values are repeatable over a wide range of time and temperature. The  
246 extended uncertainty in measurements is calculated by evaluating the maximum possible error, shown  
247 in Figure 1(c). The calculation procedure is detailed in previous work [44]. The declared expanded  
248 uncertainty was evaluated to be 5.51% using 95% confidence (coverage factor k = 2). Relative  
249 deviations (%) between the experimental viscosity of HRMO and reported studies [52–57] at varying  
250 temperatures are shown in Figure 1(c). The average absolute deviation (AAD) is 4.84% between the  
251 experimental viscosity and previously reported studies [52–57].



252

253 Figure 1: (a) Repeatability of experimental measurements; (b) Dynamic viscosity of 0.8% nanofluid  
 254 measured by the rheometer every 31 seconds; (c) Comparative analysis of experiments and the  
 255 literature [52–57], and declared expanded uncertainty [44] (shaded area).

## 256 2.5 Rheology Parameters and Multivariable Correlation

257 This research involves the application of the Ostwald-de-Waele model [58,59] to examine the flow  
 258 characteristics of hybrid nanofluids, see later equation (9). The flow behavior and consistency index are  
 259 evaluated at varying temperatures and hybrid nanomaterial concentrations. The most popular expression  
 260 to correlate the viscosity-temperature relationship of liquids is the Vogel-Fulcher-Tammann (VFT)  
 261 equation [60], which is a well-known modification of Andrade's equation [61]. In this research, the VFT  
 262 model is applied to the experimental investigations, and the fitting parameters are tabulated for  
 263 nanofluids sample. A similar methodology was also applied in a recent study by Cherecheş et al. [61]  
 264 to correlate the temperature dependence of dynamic viscosity for alumina-based nanofluids enhanced  
 265 with ionic liquids. Experimental measurements of thermophysical properties are vital for the practical  
 266 design of thermal systems. Since recent developments in nanofluid technology have suggested that the  
 267 conventional models may not be suitable for accurate predictions of temperature-dependent properties.  
 268 This deviation can be attributed to the inadvertence of temperature, nanomaterial geometry, Brownian  
 269 motion, thermophoresis, and agglomeration factors in the classical model [3,5,27]. A recently published  
 270 comprehensive review [5] on oil-based nanofluids has compiled several multivariable correlations to  
 271 predict nanofluids' viscosity (oil-based) as a function of temperature, nanomaterial concentration, shear  
 272 parameters, etc. However, this research involves the two-parameter (temperature and concentration)  
 273 correlation proposed by Vallejo et al. [50,51], which is an extension of the Vogel-Fulcher-Tammann  
 274 model [60]. Vallejo et al. [50,51] used volumetric concentrations in their research. Therefore, a  
 275 conversion equation is used to convert mass concentration (the present work) to volumetric concentration  
 276 in order to utilize Vallejo et al. [50,51] correlation. Eq. (1) represents the conversion equation from  
 277 mass concentration ( $\varphi_m$ ) to volumetric concentration to ( $\varphi_v$ ) for a hybrid nanofluid system with an  
 278 equal proportion (1:1) of nanomaterials.  $\rho_{bf}$  and  $\rho_{np}$  are the densities of base fluid and nanomaterials.  
 279 In this research, the experimental density of HRMOs at different temperatures is utilized from previous

280 study [27], while the true densities of nanomaterials are used at ambient conditions. The density data  
 281 provided by the supplier for diamond nanoparticles and graphene nanoplatelets are 3300 kg/m<sup>3</sup> and  
 282 2250 kg/m<sup>3</sup>, respectively. For instance, the mass concentrations of hybrid nonfluids (0.4, 0.8, 1.2, 1.6,  
 283 2 mass%) corresponds to 0.191, 0.382, 0.574, 0.767, 0.961 vol.%, respectively, at 298.15K.

284

$$285 \quad \varphi_v = \left[ \frac{0.5\varphi_m \times \frac{\rho_{bf}}{\rho_{np}}}{(1-0.5\varphi_m) \times \left(1 - \frac{\rho_{bf}}{\rho_{np}}\right)} \right]_D + \left[ \frac{0.5\varphi_m \times \frac{\rho_{bf}}{\rho_{np}}}{(1-0.5\varphi_m) \times \left(1 - \frac{\rho_{bf}}{\rho_{np}}\right)} \right]_{GNP} \quad (1)$$

286

## 287 2.6 Predictions via Machine Learning Algorithms

288 The application of machine learning algorithms for predictive analysis of nanofluid properties is  
 289 extensively found in recent years. The empirical correlations developed based on experimental data and  
 290 statistical inference may not yield accurate results for a wide range of nanofluids [62,63], especially  
 291 when multivariable inputs are involved. The ease of representing a physio-chemical process with data-  
 292 driven machine learning algorithms has increased in the past few years. Different algorithms were  
 293 implemented in the literature to estimate the viscosity of nanofluids, such as ANN, LSSVM, RF, and  
 294 ANFIS (Adaptive Neuro-Fuzzy Inference) [35,64].

295 In this research, the viscosity of the hybrid nanofluids is predicted with three different machine learning  
 296 algorithms, i.e., ANN, RF, and GBM (Gradient Boosting Machine), using a software tool PYTHON.  
 297 Predictions from these learning architectures are analyzed, and the performance is determined by  
 298 several error estimation metrics. ANN is considered as a black box model because it depends on the  
 299 backpropagation of randomly initialized weights to approximate solution for the targeted output.  
 300 Random Forest is an ensemble machine learning technique capable of performing regression using  
 301 multiple decision trees with a statistical technique called bagging. GBM is also an ensemble category  
 302 algorithm developed by Friedman [65], which uses multiple tree structures upon the loss function  
 303 gradient to boost its performance and optimize prediction capability [66].

304 The input parameters for the algorithms are temperature, hybrid nanomaterial concentration, and shear  
 305 rate. The output parameter is the viscosity of diamond-graphene nanoplatelets hybrid nanofluids. The  
 306 workflow detailing different processes to predict the viscosity and analyzing the predicted results is  
 307 shown in Figure 2. The experimental dataset is divided into two separate segments for training the  
 308 algorithm and testing its robustness. The total size of the experimental data is 1050, and the ratio  
 309 between the train and test dataset is set at 0.3. A standard uniform distribution is used to split the original  
 310 dataset and maintain statistical inference between the test and train data. The data set after split is  
 311 transformed onto a scale of 0.0 to 1.0 using Eq. (2) and Eq. (3). This approach is utilized for ANN only  
 312 because RF and GBM employ tree-based structure for prediction. Therefore, RF and GBM architecture  
 313 are not affected by the scale of input data. Algorithms are trained using the input training data and then  
 314 evaluated on testing data. The predictions are obtained after convergence on the train and test datasets,  
 315 based on the statistical error metrics such as coefficient of determination (R<sup>2</sup>), Root Mean Square Error  
 316 (RMSE), Mean Absolute Error (MAE), Legate and McCabe Index (LM Index, E<sub>L,M</sub>), and Willmot index  
 317 of agreement (W Index, I<sub>A</sub>), given in Eqs. (4-8), respectively.

318

319 
$$x_{std} = \frac{(x-x_{min})}{x_{max}-x_{min}} \quad (2)$$

320 
$$x_{scale} = x_{std} \times (x_{max} - x_{min}) + x_{min} \quad (3)$$

321 
$$RMSE = \sqrt{\frac{\sum_{i=1}^n (y_i - \hat{y}_i)^2}{N}} \quad (4)$$

322 
$$MAE = \frac{1}{N} \sum_{i=1}^n |y_i - \hat{y}_i| \quad (5)$$

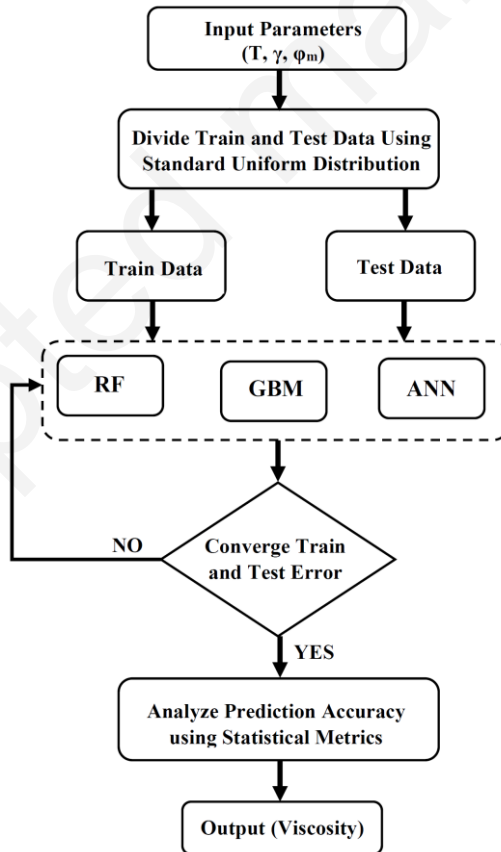
323 
$$R^2 = 1 - \frac{\sum_{i=1}^n (y_i - \hat{y}_i)^2}{\sum_{i=1}^n (y_i - \bar{y}_i)^2} \quad (6)$$

324 
$$E_{L,M} = 1 - \frac{\sum_{i=1}^N |y_i - \hat{y}_i|}{\sum_{i=1}^N |y_i - \bar{y}_i|} \quad (7)$$

325 
$$I_A = 1 - \frac{\sum_{i=1}^N (y_i - \hat{y}_i)^2}{\sum_{i=0}^N (|y_i - \bar{y}_i| + (\hat{y}_i - \bar{y}_i))^2} \quad (8)$$

326

327 where,  $\hat{y}_i$  represents the predicted values, and the number of observations is represented by N.  $y_i$  is the  
 328 given data point, and  $\bar{Y}_i$  is the mean of the given values.



329

330 Figure 2: The overall flowchart methodology used for viscosity predictions via machine learning  
 331 algorithms.

332 **3. Results and discussion**

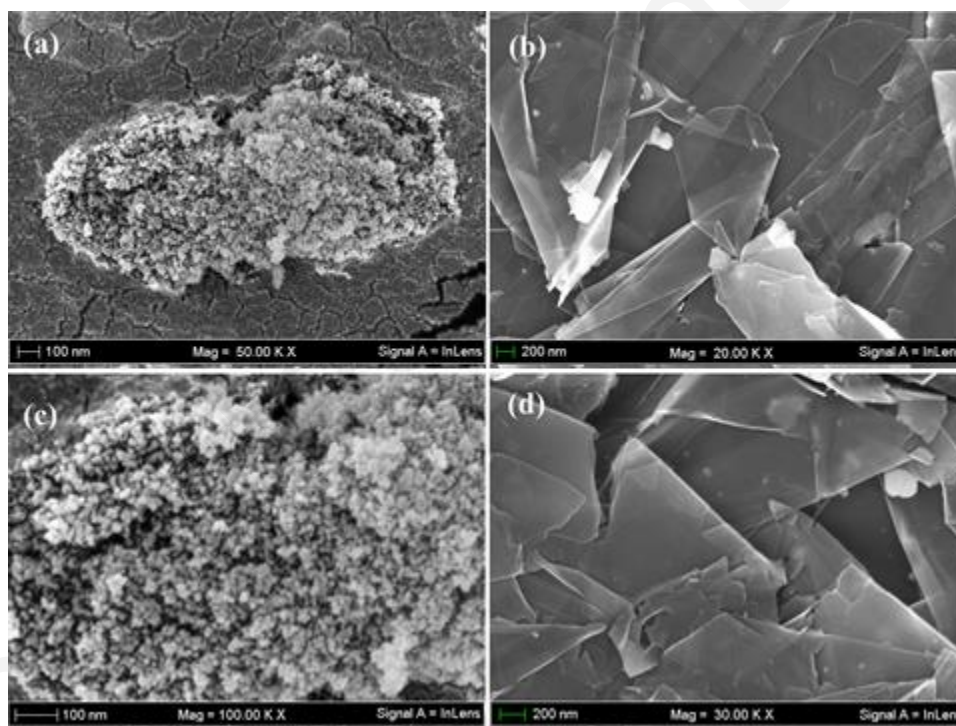
333 **3.1 Nanoparticle Characterizations**

334 **3.1.1 Electron Microscopy**

335 FESEM is used to understand the size and morphology of the nanomaterials. Micrographs of diamond  
336 nanoparticles and graphene nanoplatelets are shown in Figure 3(a, c) and (b, d), respectively. The  
337 agglomerates of diamond nanoparticles are observed. Thin layers of graphene nanoplatelets can be  
338 clearly seen in the FESEM micrograph along with some fractured surfaces.

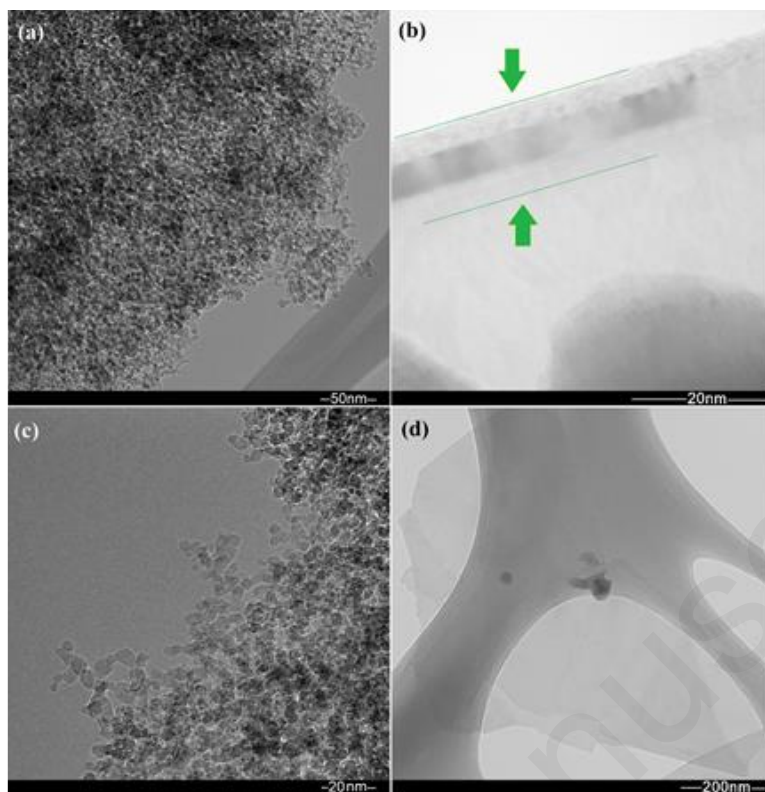
339 TEM image of diamond nanoparticles shows spherical shaped particles with a narrow and consistent  
340 size distribution, as seen in Figure 4(a, c). Some big sizes can also be seen solely due to the micro  
341 granules of diamond nanoparticles. TEM analysis in Figure 4(b, d) reveals the multiple layers of  
342 graphene nanoplatelets. Thin layered nanoplatelets of graphene can be seen in the area enclosed with  
343 arrows. TEM analysis confirms the primary particle size of diamond nanoparticles in the nanometre  
344 range and of graphene nanoplatelets in the micron range, which is in good agreement with the data  
345 provided by the supplier. The average size of diamond nanoparticles with spherical morphology is in  
346 the range of 3-10 nm, while the average thickness of graphene nanoplatelets is confirmed at 10 nm.

347



348

349 Figure 3: SEM micrographs of (a, c) Diamond nanoparticles and (b, d) Graphene nanoplatelets at  
350 different magnifications.



351

352 Figure 4: TEM images of (a, c) Diamond nanoparticle and (b, d) Graphene nanoplatelets at different  
353 magnifications.

### 354 3.1.2 Elemental Analysis

355 EDX spectroscopy is used to study the elemental composition of diamond nanoparticles and graphene  
356 nanoplatelets. Figure 5 shows the EDX analysis, and it confirms the presence of mainly Carbon (C) and  
357 Oxygen (O) in diamond nanoparticles and graphene nanoplatelets. The weight percentages of elements  
358 obtained for diamond nanoparticles are 86.88 for C, 12.97 for O, along with a negligible quantity of  
359 Chlorine (Cl). The weight percent of elements obtained from the EDX analysis of graphene  
360 nanoplatelets values 96.83% for C and 2.03% for O with minor impurities of Sulphur (S) and Nitrogen  
361 (N). EDX analysis of diamond nanoparticles and graphene nanoplatelets confirms the obtained  
362 nanomaterials are in a highly pure state.

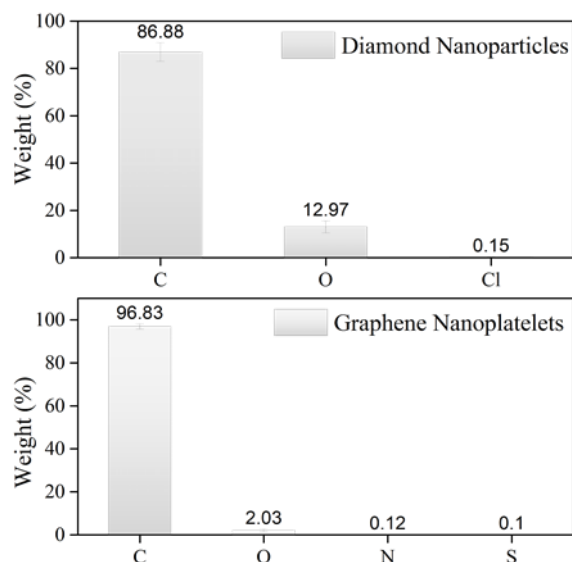


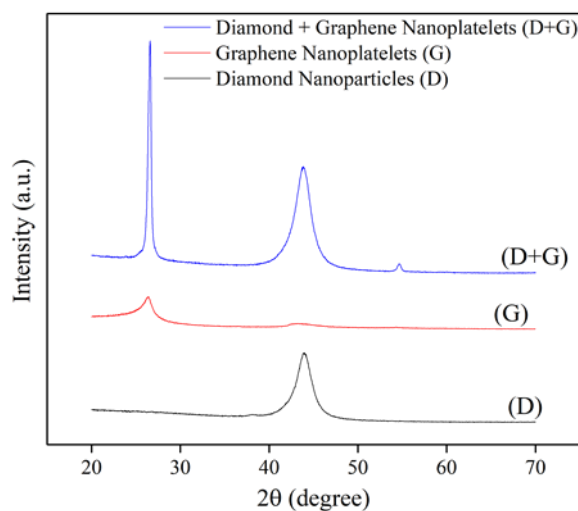
Figure 5: EDX analysis of diamond nanoparticles and graphene nanoplatelets

### 3.1.3 XRD Analysis

XRD analysis is performed on the starting nanomaterials and the obtained hybrid material. Scans of diamond nanoparticles, graphene nanoplatelets, and diamond-graphene nanoplatelets mixture are shown in Figure 6. The observed pattern of diamond nanoparticles shows a significant peak at  $2\theta = 44^\circ$  with miller indices (111), which is the characteristic peak of diamond nanoparticles [67]. The broadening of the peak is mainly due to the nano-sized crystallites. There appeared no other intense peak between  $20^\circ < 2\theta < 70^\circ$ , which confirms the purity of this starting material. The XRD scan of graphene nanoplatelets exhibits three reflections. However, the intensities of two minor peaks are compressed in Figure 6, due to the high intensity of one major peak corresponding to the graphene nanoplatelets [33]. The peak appeared at around  $2\theta = 26^\circ$  is most visible due to its intensity and two minor reflections around positions  $45^\circ$  and  $55^\circ$  suppressed due to the scale of other scans. Figure 6 also shows the XRD scan of diamond-graphene nanoplatelets, which is the hybrid material obtained through mechanical mixing of equal quantities of diamond nanoparticles and graphene nanoplatelets. The appearance of peaks in the scan of diamond-graphene nanoplatelets at similar positions, as in the scans of pure materials, confirms the successful formation of the hybrid material.

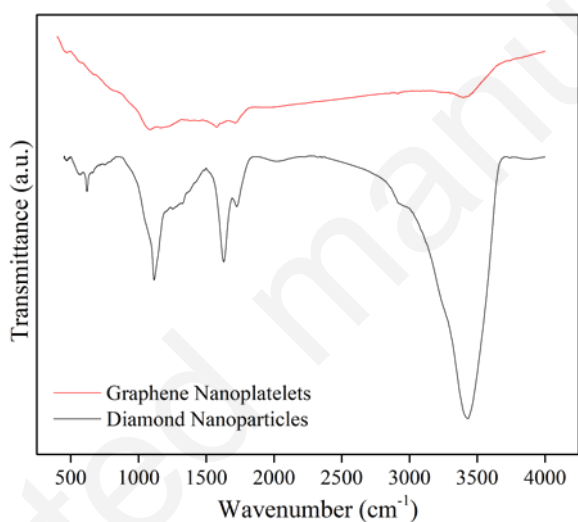
### 3.1.4 FTIR Analysis

FTIR spectra of diamond nanoparticles and graphene nanoplatelets are shown in Figure 7. The scans are performed over the wavenumber ranging from  $400$  to  $4000\text{ cm}^{-1}$ . The scan of diamond nanoparticles shows the major peak around  $3420\text{ cm}^{-1}$  which can be attributed to the stretching of  $\text{-OH}$  mode. A shouldered peak appeared around  $1700\text{ cm}^{-1}$ , which is due to the  $\text{-OH}$  bending vibration or presence of the carboxyl ( $\text{-COOH}$ ) group on the surface of diamond nanoparticles. Peaks around  $1250\text{ cm}^{-1}$  and  $1370\text{ cm}^{-1}$  correspond to the  $\text{CO}$  bending vibration and  $\text{-CH}$  bending vibration. The appearance of these two peaks can be attributed to the presence of the ester group ( $\text{CH}_3\text{-COOR}$ ). Scan of graphene nanoplatelets showed a strong adsorption peak at  $3450\text{ cm}^{-1}$ , which can be assigned to the  $\text{O-H}$  stretching. The band appeared around  $1700\text{ cm}^{-1}$  is the characteristic absorption band of  $\text{C=O}$  stretching of ketone and lactone. A band around  $1600\text{ cm}^{-1}$  can be attributed to the carboxyl group. The stretching vibration of  $\text{C-OH}$  group appeared in the form of a peak around  $1250\text{ cm}^{-1}$ .



392

393 Figure 6: XRD scans of (a) Diamond nanoparticles, (b) Graphene nanoplatelets, and (c) Diamond-  
394 Graphene nanoplatelets.



395

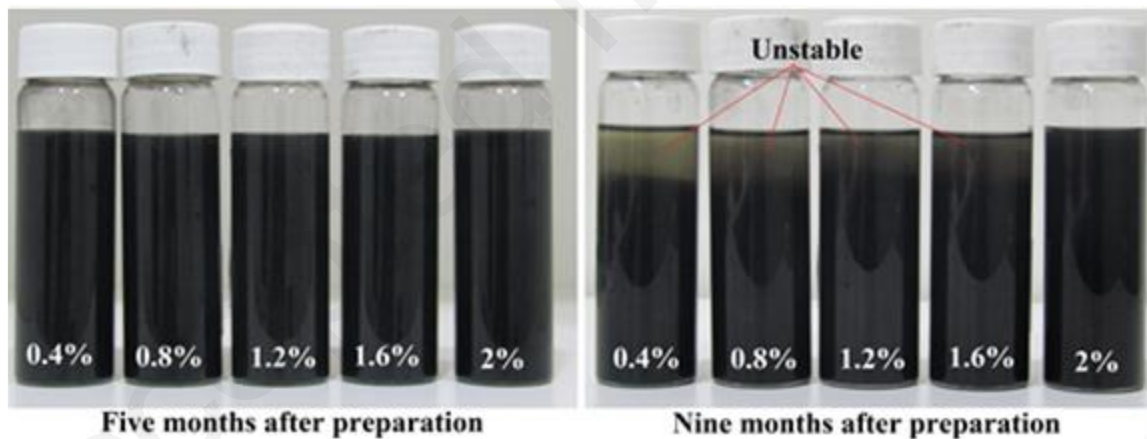
396 Figure 7: FTIR scans of diamond nanoparticles and graphene nanoplatelets

### 397 3.2 Stability of nanofluids

398 Nanofluid stability is a crucial factor in practical applications, and it is directly influenced by the nature  
399 and properties of nanomaterial and conventional fluid. The validity and effectivity of a nanosuspension  
400 depend on its stability. Therefore, the stability should be evaluated before thermophysical properties  
401 measurements or applying it in any heat transfer device. In this research, the two-step method is  
402 employed to disperse a hybrid mixture of diamond nanoparticles and graphene nanoplatelets in HRMO.  
403 Initially, the samples are prepared using ultrasonication and without surfactant. However, all the  
404 nanofluids exhibited very poor stability, and nanomaterial sediment appeared at the bottom of the glass  
405 tubes. Then, a new set of samples are prepared using a non-ionic surfactant (Span 85). After a few tests,  
406 the optimum mass concentration of hybrid nanomaterial to surfactant (Span85) ratio is fixed at 1:5. In  
407 our previous study [44] involving diamond dispersions in a similar type of oil, the optimum  
408 concentration of stabilizer was found at 1:7 (diamond:Span85). However, the required surfactant  
409 quantity in this research is found to be less due to the presence of graphene nanoplates. Graphene  
410 nanoplatelets are materials with significantly large dimensions, and they behave differently than

411 diamond nanoparticles with three-dimensional structure (all dimensions are approximately similar) or  
412 zero-dimensional (if treated as a point). Muthuraj et al. [68] prepared graphene nanoplatelets dispersions  
413 in sunflower oil using 1-hour ultrasonication to stabilize nanofluids without surfactant. In the present  
414 investigation, Span 85 provides prolonged stability to hybrid nanosuspensions. Fresh nanofluid samples  
415 are prepared with the overmentioned surfactant at five varying concentrations and subjected to static  
416 conditions at room temperature (296K). The photographs are taken after five months, and the nanofluids  
417 are found to be highly stable without any clear liquid at the top or bottom sediments, shown in Figure  
418 8. Another photograph is taken after nine months of preparation that can be visualized in Figure 8. A  
419 visible flocculated-type sediment or unstable formations are observed in all samples after nine months  
420 of preparation. The hybrid nanosuspension with a high concentration (2%) can be seen intact and  
421 dispersed in HRMO after nine months. Based on these results, it can be concluded that the hybrid  
422 nanofluids exhibit a minimum of five months stability at static and ambient conditions. Generally, the  
423 nanofluids with high nanomaterials concentration exhibit fast sedimentation compared to low  
424 concentrations. However, this research shows that the high concentration (2%) of hybrid nanofluid  
425 exhibits prolonged stability than lower concentrations after nine months. This is attributed to the  
426 packing effect in particle-liquid suspensions. The high concentration of large dimensional materials  
427 such as tubular structures or nano-sheets may behave differently than small dimensional particles.  
428 Increasing the concentration of large dimensional nanomaterials in the fluid drastically increase the  
429 viscosity due to the packing effect. A further increase in concentration leads to slurry formation until it  
430 ceases to flow. Therefore, it is possible that the high concentration of hybrid nanofluid in this research  
431 may exhibit packing effect due to the presence of graphene nanoplatelets. Thus, indicating a better  
432 stability than lower mass concentrations.

433



434

435 Figure 8: Stability evaluation of hybrid nanosuspensions in HRMO after (a) five months and (b) nine  
436 months of preparation.

### 437 3.3 Rheology Experimental Measurements

438 Fresh samples of hybrid nanosuspensions are subjected to rheology measurements at a wide range of  
439 shear rates and temperatures as described previously. The experimental results are analyzed, and the  
440 sensitivity of shear rate, temperature, nanomaterial concentration, and surfactant is discussed in the  
441 following sub-sections.

### 3.3.1 Flow Behaviour

The flow behavior of hybrid nanofluids is investigated under a shear rate range of 1-2000  $s^{-1}$  at five different temperatures. The viscosity profiles of HRMO and hybrid nanofluids (stabilized by Span 85) are presented in Figure 9(a-e). It is observed that all HRMO and all nanofluids exhibit similar viscous behavior regardless of the temperature. The viscosity is decreasing during shear ramp conditions, where a generalized decrease is observed at a low shear rate ranging between 1-100  $s^{-1}$ . The change in viscosity in the range of 100-2000  $s^{-1}$  is minimal compared to viscous values at a low shear rate. It is found that shear-thinning behavior is gradually disappearing at higher shear rates, and the nanofluid samples are tending towards Newtonian plateau, but still not completely Newtonian at the entire investigated shear range. This decrease in viscosity at increasing shear rate also suggests that the HRMO and hybrid nanofluids exhibit shear-thinning behavior, which is more profound at lower shear rates. Similar behavior was also observed by Krishnakumar et al. [69] in the case of Alumina-ethylene glycol nanofluid. Generally, the flow behaviour of HRMO depends on the chemical constituents in it. The composition, type and nature of long/short hydrocarbon chains representing paraffinic, naphthenic, and aromatic components in the oil may change the molecular thermophysical properties, molecular weight and flow behaviour of HRMOs. In this research, HRMO exhibits shear thinning behaviour and the addition of hybrid nanomaterials in HRMO at varying concentrations does not change the trend of flow behavior.

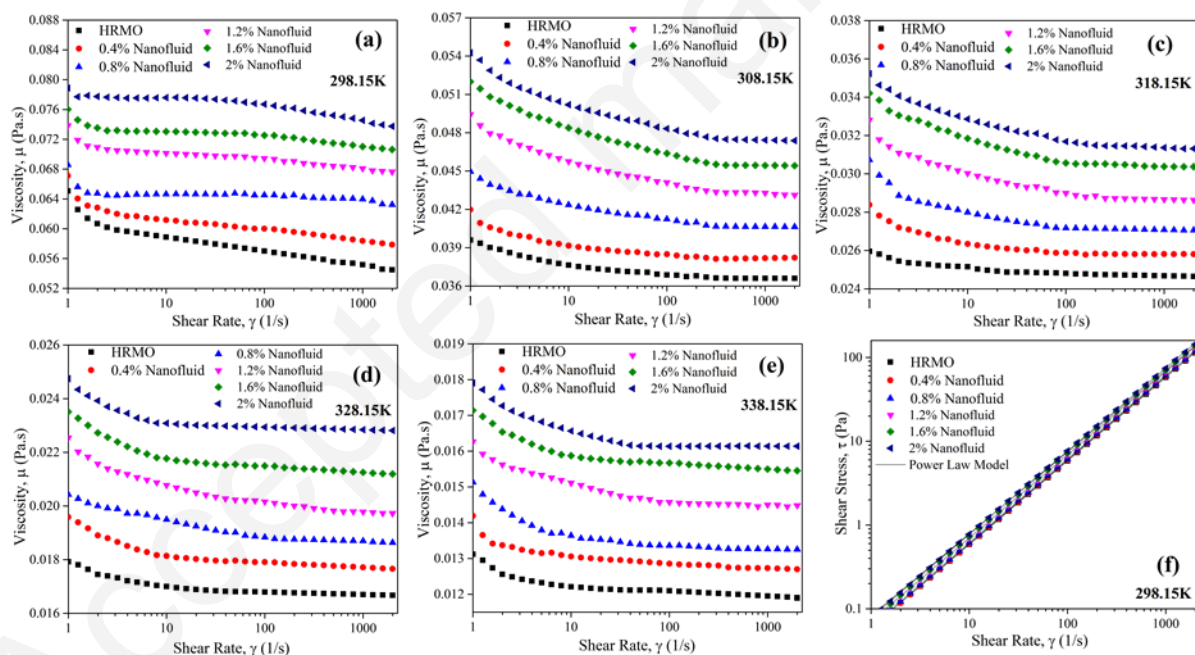


Figure 9: (a-e) The change in viscosity of HRMO and hybrid nanofluids at varying temperatures; (b) Impact of shear stress on the shear behavior, with power-law model fitting.

To further quantify the non-Newtonian character, the experimental shear stress and shear rates are plotted in the logarithmic scale, exemplified in Figure 9(f). The Ostwald-de-Waele relationship is applied to confirm the flow characteristics, given in Eq. (9). This model is also known as the power-law model to characterize fluid behavior, where  $\tau$  represents shear stress (Pa),  $\gamma$  represents shear rate ( $s^{-1}$ ),  $n$  is flow behavior index, or power-law index (-), and  $k$  is flow consistency index ( $Pa \cdot s^n$ ). An excellent data fitting of the power-law model (Ostwald-de-Waele relationship) can be seen in Figure

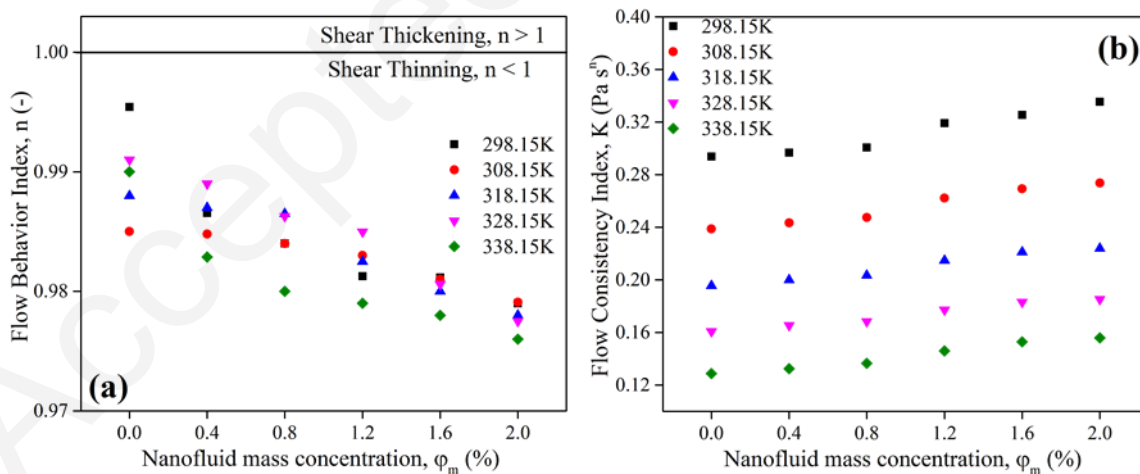
470 9(f). Initially, the logarithmic values of shear stress and shear rate are plotted, and the quantities of flow  
 471 consistency and power-law index are obtained for HRMO and hybrid nanofluids at varying  
 472 temperatures and mass concentrations. The procedure was previously applied by Cabaleiro et al. [58].  
 473 The change in the values of  $n$  is the deciding parameter to characterize the nature of nanofluid flow  
 474 behaviour. If  $n = 1$ , the flow behaviour can be termed as Newtonian. However, if the values of  $n$  are  
 475  $>1$  or  $<1$ , then the fluid can be categorized non-Newtonian with shear thickening or shear thinning  
 476 characteristics, respectively. The evaluated values of  $n$  and  $k$  from the logarithmic relationship between  
 477 shear stress and shear rate are shown in Figure 10(a) and (b), respectively. HRMO and nanofluids  
 478 exhibit  $n < 1$  at all conditions, which confirms the shear-thinning character of fluid. A generic  
 479 decreasing trend of  $n$  is observed by increasing temperature and hybrid nonmaterial mass concentration.  
 480 This analysis concluded that the hybrid nanofluid flow is shifting away from the Newtonian plateau if  
 481 the concentration of diamond-graphene nanoplatelets in HRMO is increased. Figure 10(b) presents flow  
 482 consistency index  $k$  at varying temperatures and hybrid nanomaterial concentrations. It is observed that  
 483  $k$  is increasing with nanofluid mass concentration. However, an inverse relationship is observed with  
 484 temperature. The increase in  $k$  values for hybrid nanofluids can be attributed to the nature of  
 485 nanomaterials. Generally, the presence of nanomaterials in the fluid resists the shear flow due to  
 486 nanomaterial geometry and dispersion characteristics. It may lead to an increase in viscosity, and thus,  
 487 the consistency index is also increased. The reduction in  $k$  with enhancing temperature can be attributed  
 488 to the minimizing interactions among molecules and increasing intermolecular distance leading to lower  
 489 viscosity and consistency index. Similar behavior for power-law index and flow consistency index was  
 490 also reported in the literature [70] for hybrid nanofluids containing Ag-Fe<sub>3</sub>O<sub>4</sub> dispersions in ethylene  
 491 glycol/water.

492

493

$$\tau = k\gamma^n \quad (9)$$

494



495

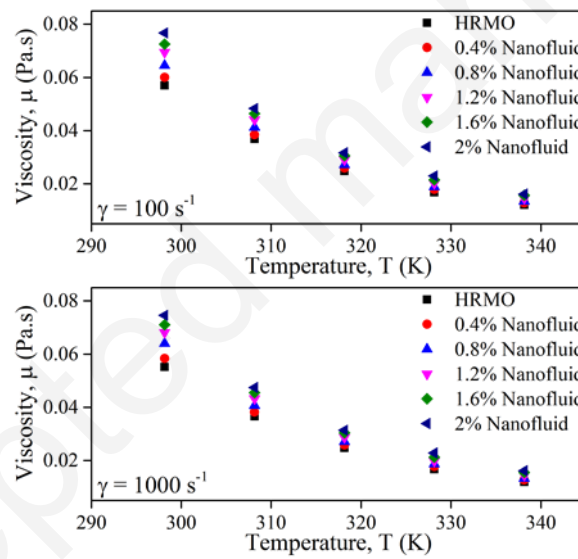
496 Figure 10: Flow characteristics, (a) flow behavior index, and (b) flow consistency index, of diamond-  
 497 graphene nanoplatelets at varying temperatures and mass concentrations.

### 498 3.3.2 Impact of Temperature

499 Viscosity is a temperature-dependent property, and it is important to understand the flow characteristics  
 500 of HRMO and hybrid nanofluids at different temperatures for their usage in practical applications. The

501 investigations are carried out at five different temperatures. Figure 11 exemplifies the nanosuspension  
 502 viscosity at a constant shear rate. A typical trend of viscosity-decrement can be seen, which is attributed  
 503 to intermolecular bond attenuation at high temperatures. An average of 79% decrement in viscosity is  
 504 observed from 298.15K to 338.15K. Interestingly, the average viscosity difference between HRMO and  
 505 hybrid nanofluids becomes smaller with the increase in temperature, evident from Figure 11. This  
 506 phenomenon can be attributed to the increase in kinematic energy of nanomaterials suspended in the  
 507 fluid at higher temperatures, which may reduce the resistance to flow and orient the nanomaterials in  
 508 the direction of flow.

509 It is a noteworthy fact that the stochastic motion of randomly moving hybrid nanomaterials in a  
 510 suspension is directly influenced by temperature, which results in a change in the viscous behavior of  
 511 nanofluid. The presence of graphene nanoplatelets in the suspension along with a spherical-type  
 512 diamond nanoparticle can have an interesting and different viscous phenomenon compared to mono-  
 513 nanomaterial-based nanofluids. Since graphene nanoplatelets have a sheet-type structure and huge  
 514 dimensions compared to diamond nanoparticles, both nanomaterials may co-exist in a much higher  
 515 interaction due to entanglement and high surface area. The Brownian motion of nanomaterials increases  
 516 at elevated temperatures, which directly impacts thermophysical properties [68]. The large dimension  
 517 of these nanoplatelets may tend them to fold during Brownian motion, which can change the viscous  
 518 behavior.



519

520 Figure 11: Viscosity of diamond-graphene nanoplatelets hybrid nanofluids at varying temperatures.

521 Temperature-dependent viscosity can be modeled using the Vogel-Fulcher-Tammann (VFT) model,  
 522 widely used in the literature [50,51,71]. The model is expressed in Eq. (10).

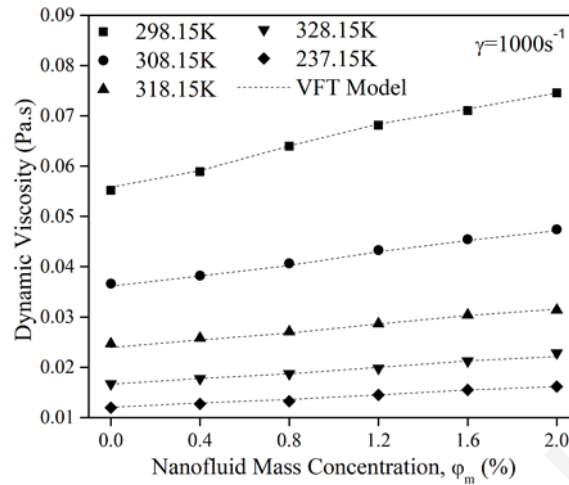
523

$$524 \quad \mu = \mu_o \cdot e^{\frac{A}{T-T_o}} \quad (10)$$

525

526 where,  $\mu_o$ ,  $A$  and  $T_o$  are constants and can be adjusted. Viscosity values are not constant, even at higher  
 527 shear rates. Therefore, fitting parameters are evaluated at four different shear rate conditions, i.e., 100  
 528  $s^{-1}$ , 500  $s^{-1}$ , 1000  $s^{-1}$ , and 2000  $s^{-1}$ . The corresponding values at varying hybrid nanofluid concentrations

529 and error estimation between experimental and Eq. (10) are tabulated in Table 1. AAD, SSE, and  $R^2$  in  
 530 Table 1 correspond to average absolute deviation (%), the sum of squared error, and coefficient of  
 531 determination, respectively. Figure 12 exemplifies and confirms that Eq. (10) can be used to model  
 532 temperature-dependent viscosity of hybrid nanofluids at varying concentrations.



533  
 534 Figure 12: The comparison of experimental data with Eq. (10) at a constant shear rate of 1000 s<sup>-1</sup>.

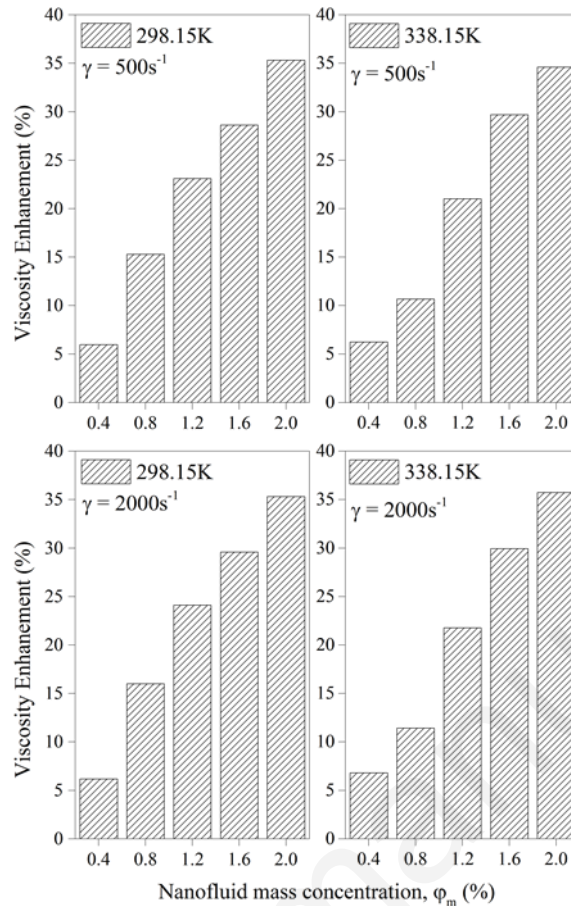
535 Table 1: Adjustable parameters of Eq. (10) and error evaluation at four different shear rates.

Shear Rate 100 s <sup>-1</sup>						
Concentration (%)	0	0.4	0.8	1.2	1.6	2
$\mu_o$ (Pa·s) ×10 <sup>-5</sup>	4.768	5.34	5.58	5.9	6.58	6.51
A (K)	1000.64	1000.62	1000.65	1000.66	1000.56	1000.71
T <sub>o</sub> (K)	157.52	156.08	156.3	156.63	155.33	156.66
AAD (%)	0.22	0.82	0.93	0.37	0.31	0.85
SSE (Pa·s) ×10 <sup>-6</sup>	2.95	1.39	0.58	0.32	0.28	0.58
R <sup>2</sup> (%)	99.95	99.96	99.97	99.98	99.98	99.97
Shear Rate 500 s <sup>-1</sup>						
Concentration (%)	0	0.4	0.8	1.2	1.6	2
$\mu_o$ (Pa·s) ×10 <sup>-5</sup>	4.78	5.3	5.52	5.89	6.57	6.85
A (K)	1000.64	1000.98	1001.01	1001.01	1000.91	996.27
T <sub>o</sub> (K)	157.34	155.99	156.33	156.36	155.08	155.83
AAD (%)	0.37	1.14	0.88	0.364	0.11	0.81
SSE (Pa·s) ×10 <sup>-6</sup>	1.39	3.07	0.3	0.12	0.54	0.51
R <sup>2</sup> (%)	99.88	99.93	99.98	99.98	99.99	99.97
Shear Rate 1000 s <sup>-1</sup>						
Concentration (%)	0	0.4	0.8	1.2	1.6	2
$\mu_o$ (Pa·s) ×10 <sup>-5</sup>	4.78	5.46	5.62	6	6.64	6.89
A (K)	1000.62	996.27	996.47	996.47	996.69	996.65
T <sub>o</sub> (K)	157.161	155.849	156.557	156.582	155.351	155.498
AAD (%)	0.274	1.38	0.917	0.456	0.264	0.849
SSE (Pa·s) ×10 <sup>-6</sup>	2.25	0.279	0.365	0.206	0.189	0.597
R <sup>2</sup> (%)	99.97	99.89	99.91	99.98	99.99	99.97
Shear Rate 2000 s <sup>-1</sup>						
Concentration (%)	0	0.4	0.8	1.2	1.6	2
$\mu_o$ (Pa·s) ×10 <sup>-5</sup>	4.89	5.49	5.29	5.98	6.57	6.96
A (K)	1000.56	996.65	999.09	998.38	998.31	998.67
T <sub>o</sub> (K)	156.46	155.51	157.77	156.26	155.34	154.78
AAD (%)	0.39	1.62	1.1	0.52	0.42	0.93
SSE (Pa·s) ×10 <sup>-6</sup>	1.32	3.34	4.08	0.29	0.57	0.82
R <sup>2</sup> (%)	99.98	99.84	99.93	99.98	99.98	99.97

### 537 **3.3.3 Impact of Nanomaterial Mass Concentration**

538 The concentration of nanofluids plays a vital role in designing thermal applications. The thermal  
539 properties of the fluid can be elevated by increasing the quantity of nanomaterials. However, the  
540 viscosity can also shoot up at high concentrations, which may adversely impact on the thermal  
541 performance of the system. Therefore, the quantity of nanomaterials in conventional fluid must be  
542 optimized. There is a consensus among the reported studies that the viscous parameter is directly  
543 proportional to the amount of dispersed nanomaterials in the liquid. In this research, nanofluids are  
544 experimentally tested at five varying mass concentrations. Figure 13 represents the percentage increase  
545 in viscosity of hybrid nanofluids compared to HRMO at temperatures 298.15K and 338.15K, and shear  
546 rates  $500 \text{ s}^{-1}$  and  $2000 \text{ s}^{-1}$ . An increasing trend in hybrid nanofluid viscosity is observed at all  
547 investigated conditions. It is observed that the lower mass concentration (0.4%) constitutes an average  
548 6% enhancement in viscosity. However, the highest mass concentration exhibits an average 35%  
549 elevation in viscosity. Similar trends are observed at different shear rates and temperature conditions  
550 for all samples. This increase is attributed to diamond and graphene nanoplatelets in HRMOs that act  
551 as a solid particle and sheets-type structure, respectively. It provides extra resistance among the different  
552 folds of fluid media layers at the molecular level. This extra resistance results in a reducing flow  
553 character and hence, increasing the viscosity of the fluid. It is crucial to mention that two-dimensional  
554 nanomaterial under Brownian motion exhibit entanglement behavior. The movement of sheet-type  
555 nanomaterials is multi-directional in the fluid medium that can influence the viscosity.

556 A comparison of this investigation and our previous works [27,29,44,72] involving similar base fluid  
557 is presented in Figure 14 to state the position of diamond-graphene nanoplates hybrid nanofluids among  
558 mono-nanoparticle based nanofluid systems. It is observed that nanofluids containing MWCNTs in oil  
559 [72] have a relatively high increment in viscosity compared to hybrid nanosuspension. A generic  
560 comparison of hybrid nanofluids with diamond-oil nanosuspensions [44] suggests minimal difference  
561 in viscosity enhancement. However, oil-based nanosuspension containing functionalized metallic oxide  
562 nanoparticles constitutes lower viscosity enhancement than hybrid nanofluids under investigation.



563

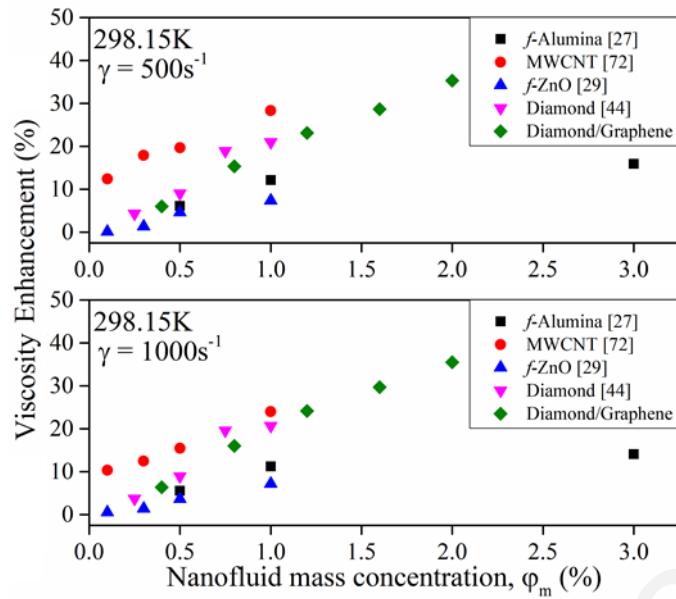
564

Figure 13: Impact of diamond-graphene nanoplatelets hybrid nanofluid concentration.

565

### 566 3.3.3 Impact of Surfactant

567 The addition of surfactants can alter the rheology of nanofluids [47]. In this research, hybrid nanofluids  
 568 are prepared using a non-ionic surfactant, i.e., Span 85. The mass concentration of hybrid nanomaterial  
 569 to surfactant (Span85) ratio is fixed at 1:5. A new sample is prepared with HRMO mix with Span 85  
 570 and without hybrid nanomaterial to analyze the impact of surfactant. The surfactant quantity in the new  
 571 sample is set equivalent to 2% nanofluid but without hybrid nanomaterials. This sample is named  
 572 HRMO+Span85(1:5). The comparative results of pure HRMO, HRMO+Span85(1:5), and 2% nanofluid  
 573 are compared in Figure 15 at two different shear rates. An interesting phenomenon is observed, HRMO  
 574 viscosity is slightly increased by adding surfactant alone. Similar behavior is observed at all temperature  
 575 conditions. Relative viscosities for HRMO+Span85(1:5) and 2% nanofluid compared to HRMO are  
 576 evaluated and presented in Figure 15(b). It is observed that HRMO+Span85(1:5) exhibits an  
 577 enhancement in the range of 7.8% to 14.9% at varying temperatures, where 14.9% is observed that  
 578 338.15K. However, the viscosity enhancement for 2% nanofluid is in the range of 27-35%, where the  
 579 maximum increase is found at 338.15K. It can be concluded from this comparative study that the  
 580 quantity of surfactant directly influences the viscous properties of hybrid nanofluids by a wide margin.

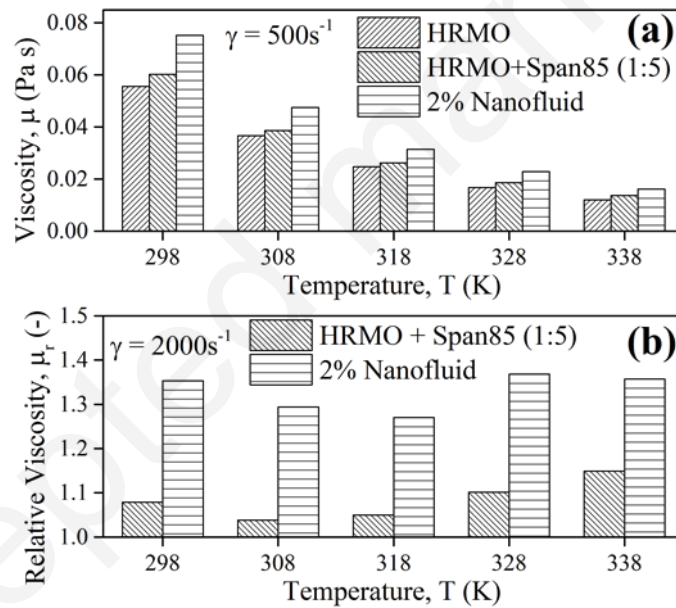


581

582

583

Figure 14: Comparative analysis of viscosity enhancement of hybrid nanofluids compared to the literature [27,29,44,72] using similar base fluid.



584

585

Figure 15: Influence of surfactant on the viscosity of HRMO and nanofluid at varying temperatures.

586

### 3.4 Two-Variable Correlation

587

588

589

590

591

592

593

594

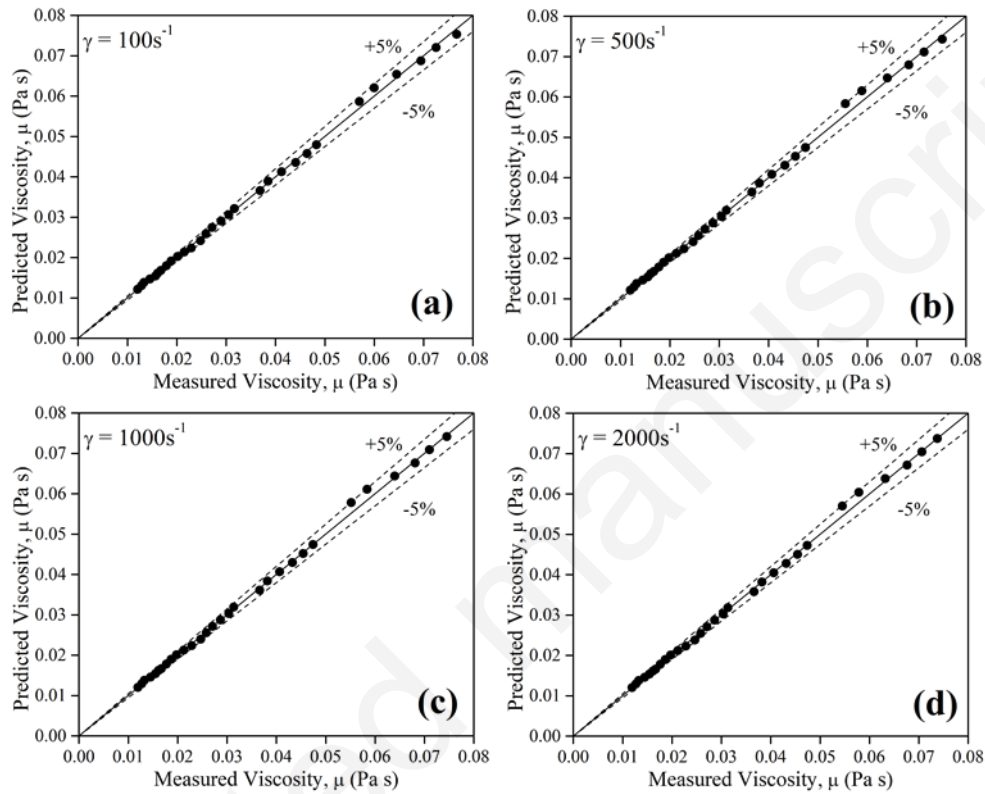
A generalized two-variable correlation is developed to express viscosity of diamond-graphene nanoplatelets based hybrid nanosuspension as a function of temperature and hybrid nanomaterial volumetric concentration. Eq. 1 is utilized to convert mass concentration to volumetric concentration. The correlation equation is given in Eq. (11). The generic form of this correlation is taken from the studies performed by Vallejo et al. [50,51]. The correlation is applied to four different shear rates, i.e.,  $100 \text{ s}^{-1}$ ,  $500 \text{ s}^{-1}$ ,  $1000 \text{ s}^{-1}$ , and  $2000 \text{ s}^{-1}$ . The parity plots are presented in Figure 16, and the fitting parameters, along with the error estimations, are tabulated in Table 2. It is found that the predicted values from Eq. (11) are under  $\pm 5\%$  mean absolute error. The new coefficients of adjustable parameters considering

595 temperature and concentration are presented in Table 2. Here,  $\mu_o$ ,  $A$  and  $T_o$  are fixed for the base fluid  
 596 and can be referred to Table 1.

597

$$598 \quad \mu = \mu_o \cdot e^{\frac{A}{T-T_o}} + B\phi_v \cdot e^{c/T} - D\phi_v^2 \quad (11)$$

599



600

601 Figure 16: Parity plots for the comparative analysis of experimental data and Eq. (11) at (a)  $100 \text{ s}^{-1}$ ,  
 602 (b)  $500 \text{ s}^{-1}$ , (c)  $1000 \text{ s}^{-1}$  and (d)  $2000 \text{ s}^{-1}$ .

603 Table 2: Adjustable parameters of Eq. (11) and error evaluation at four different shear rates.

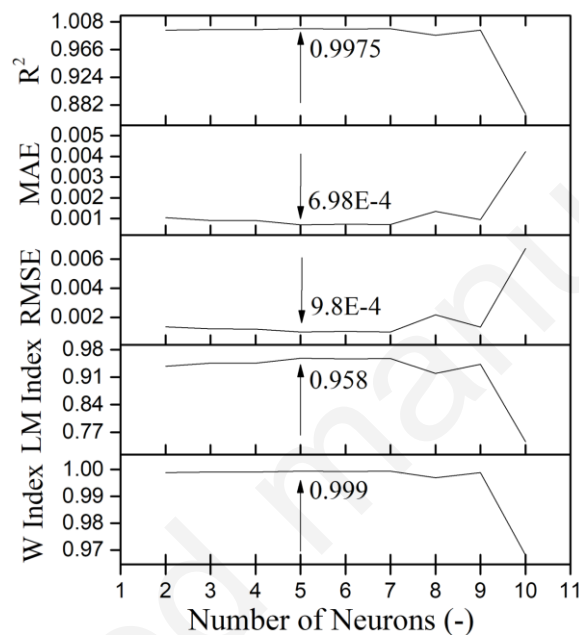
Shear rate ( $\text{s}^{-1}$ )	100	500	1000	2000
$B \text{ (Pa}\cdot\text{s)} \times 10^{-7}$	3.343	3.343	3.343	3.343
$C \text{ (K)}$	3246.482	3227.738	3235.095	3246.609
$D \text{ (Pa}\cdot\text{s)} \times 10^{-4}$	6.357	2.155	2.616	5.323
AAD (%)	1.17	1.23	1.16	1.28
SSE ( $\text{Pa}\cdot\text{s)} \times 10^{-5}$	1.3	1.81	1.69	1.65
$R^2$ (%)	99.88	99.84	99.85	99.85

604

### 605 3.5 Predictions via Machine Learning Algorithms

606 Three different algorithms are applied to predict the viscosity of hybrid nanofluids as a function of three  
 607 input variables (temperature, mass concentration, and shear rate). The comparative error matrix for  
 608 these three algorithms is compared in Table 3. At first, the ANN algorithm is trained iteratively to select  
 609 the best possible hyperparameters such as the number of neurons, number of hidden layers, activation

610 function, number of iterations, and learning rate of the algorithm. A grid search is performed within a  
 611 range of parameters to evaluate the optimum parameter. Rectified Linear Unit (ReLU) is set as the  
 612 activation function with five number of hidden layers. The optimized architecture of ANN is found at  
 613 five neurons at a learning rate of 0.01, as shown in Figure 17. Xavier initialization is used to evenly  
 614 initiate the weights to avoid local minima and vanishing gradient problem. Gradient descent is used as  
 615 an optimization algorithm, and the algorithm performance on train and test datasets are monitored to  
 616 prevent overfitting. An optimum number of neurons are selected at 5 in each layer to achieve a balanced  
 617 trade-off between the error metrics utilized in this study. The train and test data are plotted in Figure  
 618 18(a) and (b), respectively. A good agreement between the experimental viscosity and ANN predictions  
 619 are observed.



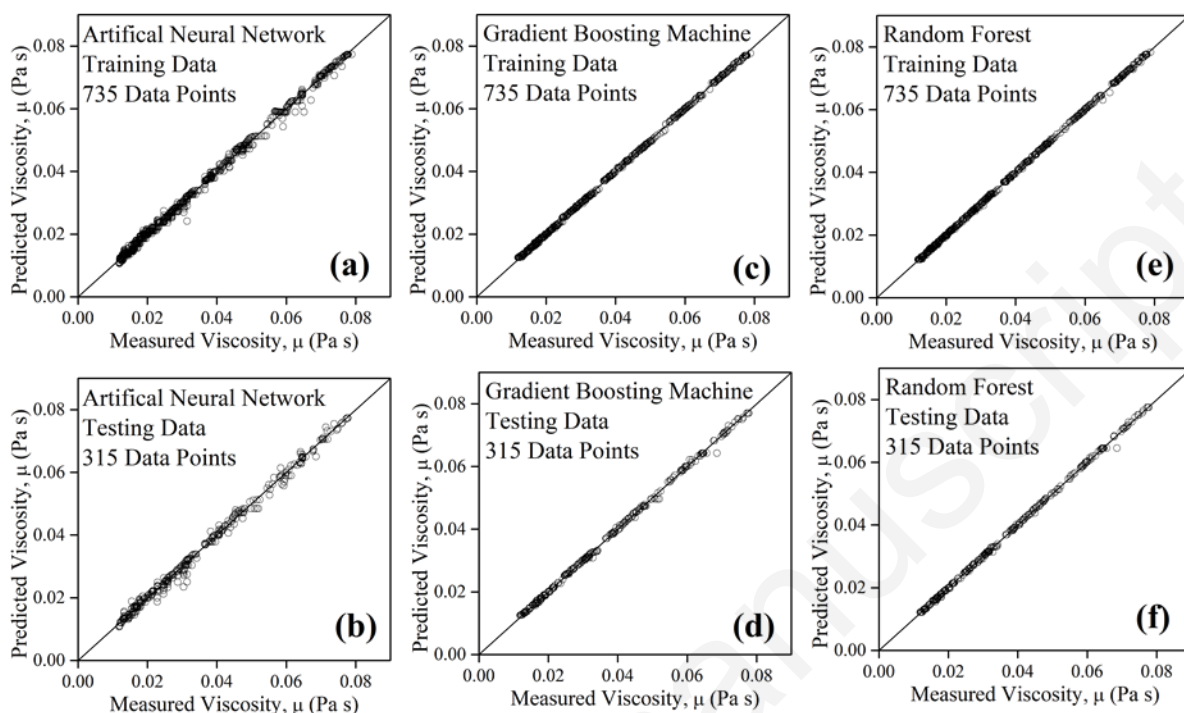
620

621 Figure 17: Error analysis to find an optimum number of neurons for ANN predictions of hybrid  
 622 nanofluid viscosity.

623 GBM is applied as a second algorithm to predict hybrid nanofluid viscosity. Figure 18(c) and (d)  
 624 presents the observed and the predicted values for the train and test dataset for GBM. The coefficient  
 625 of determination  $R^2$  is observed to be 0.99 for both datasets, and other error metrics are monitored lower,  
 626 as shown in Table 3. The learning rate for GBM is set at 0.5 with a maximum depth of 50. The number  
 627 of estimators is selected as 10 with a loss function of mean squared error. All hyperparameters are  
 628 iteratively chosen for optimum performance. The  $R^2$  for the train and testing data exhibit a 0.99 value,  
 629 while other error metrics for both datasets are relatively similar. It shows that GBM can predict the  
 630 viscosity of nanofluids with high precision. It is observed from Figure 18(c) and (d) that some predicted  
 631 values deviate from the reference equality line at approximately 0.05 Pa·s and 0.07 Pa·s. However, a  
 632 dense data cloud is observed at the reference equality line below 0.05 Pa·s.

633 The predictions for RF algorithms for train and test datasets are plotted in Figure 18(e) and (f). An  
 634 excellent prediction pattern is observed in the case of RF algorithm. The hyperparameters for RF are  
 635 iteratively selected. The number of estimators is 10, and the minimum leaf split is set at 2. The  
 636 performance of both data segments is almost similar, which concludes that RF can simulate the

637 dynamics of the nanofluids with excellent precision. The  $R^2$  for both train and testing data are identical,  
 638 i.e., 0.99.



639  
 640 Figure 18: Parity plots for predictions of training and testing data using (a, b) ANN, (c, d) GBM, and  
 641 (e, f) RF algorithms.

642 The evaluated error for ANN, GBM, and RF is summarized in Table 3. It can be deduced from the  
 643 comparative error matrix that the performance of all three algorithms on both testing and training is  
 644 very similar. It concludes the potential of machine learning algorithms in predicting the viscosity of  
 645 hybrid nanofluids based on multi-input parameters. It is found that ANN predictions exhibit slight  
 646 deviations in training and testing data, while GBM and RF do not show such considerable deviations.  
 647 Overall, RF algorithm outperforms all other algorithms and is the suitable machine learning method for  
 648 the dataset obtained in this investigation.

649 Table 3: A comparative error analysis for machine learning algorithms

Errors	ANN		RF		GBM	
	Train	Test	Train	Test	Train	Test
$R^2$	0.9983	0.9976	0.9998	0.9993	0.9997	0.9991
MAE	0.0005	0.0006	0.0001	0.0002	0.0002	0.0003
RMSE	0.0007	0.0008	0.0002	0.0004	0.0003	0.0005
$E_{L,M}$	0.9656	0.9581	0.9891	0.9819	0.9849	0.9765
$I_A$	0.9995	0.9994	0.9999	0.9998	0.9999	0.9997

650  
 651 **4. Conclusions**

652 This research involves an experimental evaluation of rheological parameters of hybrid nanosuspensions  
653 containing diamond nanoparticles and graphene nanoplatelets (1:1) in highly refined mineral oil  
654 (HRMO). The investigation is performed at varying mass concentrations (0-2 mass%) and temperatures  
655 (298.15-338.15K). The nanofluids are prepared using the two-step method involving ultrasonication  
656 and surfactant addition. Characterizations are performed for nanomaterials, which confirm the primary  
657 size, elemental composition, and high purity. The stability of nanosuspensions is evaluated for five  
658 months, and no sediment is observed. The rheological characteristics conclude that a shear-thinning  
659 non-Newtonian behavior is found, and the flow behavior index for all samples at varying temperatures  
660 is  $<1$ . The non-Newtonian behavior can be well-described by the Ostwald-de-Waele model. The  
661 sensitivity of temperature on viscous behavior shows an average of 79% decrement in viscosity from  
662 298.15K to 338.15K. VFT model is used to express temperature-dependent viscosity of HRMO and  
663 hybrid nanofluids, and fitting parameters are presented. A maximum of 35% increase in viscosity of  
664 hybrid nanosuspension is observed at the highest concentration of 2%. It is also observed that the  
665 addition of Span 85 in HRMO-based nanofluids increases the overall viscosity by a maximum of 14%.  
666 A generalized two-variable correlation is used to express viscosity as a function of temperature and  
667 hybrid nanofluid concentration with an excellent agreement. Finally, three machine learning algorithms  
668 are finally applied to predict the viscosity of hybrid nanosuspensions based on three input parameters.  
669 RF algorithm shows excellent predictions compared to GBM and ANN, which shows the potential of  
670 artificial intelligence in predicting the thermophysical properties of nanosuspensions.

671 A complete understanding of complex fluid's rheological behaviour is extremely intricate due to the  
672 known and unknown phenomenon occurring at the molecular level, such as this investigation. This  
673 research is focused on the rheology of stabilized Diamond-Graphene nanoplatelets in HRMO, which  
674 has significant potential in opening new horizons in the field of nanofluids, especially complex systems  
675 having two nanomaterials with different structures and properties. The authors intend to highlight that  
676 the increase in the hybrid nanofluids' viscosity might not be suitable for an ideal heat transfer fluid.  
677 Therefore, a detailed experimental analysis should be performed on other thermophysical properties to  
678 see a complete narrative of heat transfer and other applications. The authors propose to expand the  
679 research towards a detailed experimental architecture, including other stability methods and  
680 thermophysical properties. This research can be counted as a further step towards long-term stability  
681 and hybrid nanofluid-based structure-condition-property relationship.

## 682 **Nomenclature**

683	$A$	Adjustable parameter in Eq. 10 (K)
684	$B$	Adjustable parameter in Eq. 11 (Pa·s)
685	$C$	Adjustable parameter in Eq. 11 (K)
686	$D$	Adjustable parameter in Eq. 11 (Pa·s)
687	$E_{LM}$	Legate and McCabe Index, LM Index (-)
688	$I_A$	Willmot index of agreement, W Index (-)
689	$k$	Flow consistency index (Pa·s <sup><math>n</math></sup> )
690	$n$	Flow behavior index (-)
691	$N$	Number of observations in Eq. (4)-(8)
692	$R^2$	Coefficient of determination (-)
693	$T$	Temperature (K)
694	$T_o$	Adjustable parameter in Eq. 10 (K)
695	$x$	Input data value in Eq. (2) and (3)
696	$y_i$	Given data point in Eq. (4)-(8)
697	$\hat{y}_i$	Predicted values in Eq. (4)-(8)

698  $\bar{Y}_i$  Mean of the given values in Eq. (4)-(8)

699 **Greek Symbols**

700  $\varphi$  Nanomaterial concentration (%)

701  $\rho$  Density (kg/m<sup>3</sup>)

702  $\gamma$  Shear rate (1/s)

703  $\tau$  Shear stress (Pa)

704  $\mu$  viscosity (Pa·s)

705  $\mu_o$  Adjustable parameter in Eq. 10 (Pa·s)

706  $\mu_r$  Relative viscosity (-)

707 **Abbreviations**

708 AAD Average Absolute Deviation

709 ANN Artificial Neural Network

710 GBM Gradient Boosting Machine

711 RF Random Forest

712 HRMO Highly Refined Mineral Oils

713 EOR Enhanced Oil Recovery

714 PSO Particle Swarm Optimization

715 RBF Radial Basis Function

716 LSSVM Least-square Support Vector Machine

717 VFT Vogel-Fulcher-Tammann Model

718 RMSE Root Mean Square Error

719 MAE Mean Absolute Error

720 SSE Sum of Squared Error

721 **Subscripts**

722 *np* Nanoparticle

723 *bf* Basefluid

724 *v* Volume

725 *m* Mass

726 *std* Standard deviation of input data in Eq. (2) and (3)

727 *Scale* Scaled input data in Eq. (2) and (3)

728 *min* Minimum value of input data in Eq. (2) and (3)

729 *max* Maximum value of input data in Eq. (2) and (3)

730

731 **Authorship Contribution Statement**

732 **SU Ilyas:** Conceptualization, Methodology, Validation, Formal analysis, Investigation, Writing -  
733 Original Draft. **S Ridha:** Investigation, Resources, Writing - Review & Editing, Project administration,  
734 Funding acquisition. **S Sardar:** Validation, Formal analysis, Investigation, Writing - Original Draft. **P**  
735 **Estellé:** Conceptualization, Methodology, Investigation, Writing - Review & Editing. **A Kumar:**  
736 Software, Formal analysis, Writing - Original Draft. **R Pendyala:** Conceptualization, Methodology,  
737 Resources, Writing - Review & Editing.

738 **Declaration of Competing Interests**

739 The authors declare that they have no known competing financial interests or personal relationships  
740 that could have appeared to influence the work reported in this paper.

741 **Acknowledgment**

742 This work is supported by the Institute of Hydrocarbon Recovery at Universiti Teknologi PETRONAS.  
743 The financial assistance is provided by Yayasan UTP (Grant No. YUTP 015LC0-101).

744

## 745 References

- 746 [1] R. Taylor, S. Coulombe, T. Otanicar, P. Phelan, A. Gunawan, W. Lv, G. Rosengarten, R.  
747 Prasher, H. Tyagi, Small particles, big impacts: A review of the diverse applications of  
748 nanofluids, *J. Appl. Phys.* 113 (2013) 011301. doi:10.1063/1.4754271.
- 749 [2] K. Khanafer, K. Vafai, A review on the applications of nanofluids in solar energy field, *Renew.*  
750 *Energy.* 123 (2018) 398–406. doi:10.1016/j.renene.2018.01.097.
- 751 [3] M.H. Buschmann, NANOUP TAKE - An European network on nanofluid research, in: 2018.  
752 doi:10.14311/tpfm.2018.004.
- 753 [4] D. Amin, R. Walvekar, M. Khalid, M. Vaka, N.M. Mubarak, T.C.S.M. Gupta, Recent Progress  
754 and Challenges in Transformer Oil Nanofluid Development: A Review on Thermal and  
755 Electrical Properties, *IEEE Access.* 7 (2019) 151422–151438.  
756 doi:10.1109/ACCESS.2019.2946633.
- 757 [5] A. Asadi, S. Aberoumand, A. Moradikazerouni, F. Pourfattah, G. Żyła, P. Estellé, O. Mahian,  
758 S. Wongwises, H.M. Nguyen, A. Arabkoohsar, Recent advances in preparation methods and  
759 thermophysical properties of oil-based nanofluids: A state-of-the-art review, *Powder Technol.*  
760 352 (2019) 209–226. doi:10.1016/j.powtec.2019.04.054.
- 761 [6] J. Fal, O. Mahian, G. Żyła, Nanofluids in the Service of High Voltage Transformers: Breakdown  
762 Properties of Transformer Oils with Nanoparticles, a Review, *Energies.* 11 (2018) 2942.  
763 doi:10.3390/en11112942.
- 764 [7] B. Peng, L. Zhang, J. Luo, P. Wang, B. Ding, M. Zeng, Z. Cheng, A review of nanomaterials  
765 for nanofluid enhanced oil recovery, *RSC Adv.* (2017). doi:10.1039/c7ra05592g.
- 766 [8] N.A.C. Sidik, H.A. Mohammed, O.A. Alawi, S. Samion, A review on preparation methods and  
767 challenges of nanofluids, *Int. Commun. Heat Mass Transf.* 54 (2014) 115–125.  
768 doi:10.1016/j.icheatmasstransfer.2014.03.002.
- 769 [9] R. Saidur, K.Y. Leong, H.A. Mohammed, A review on applications and challenges of  
770 nanofluids, *Renew. Sustain. Energy Rev.* 15 (2011) 1646–1668. doi:10.1016/j.rser.2010.11.035.
- 771 [10] O. Mahian, A. Kianifar, S.A. Kalogirou, I. Pop, S. Wongwises, A review of the applications of  
772 nanofluids in solar energy, *Int. J. Heat Mass Transf.* 57 (2013) 582–594.  
773 doi:10.1016/j.ijheatmasstransfer.2012.10.037.
- 774 [11] X. Cui, C. Li, Y. Zhang, D. Jia, Y. Zhao, R. Li, H. Cao, Tribological properties under the  
775 grinding wheel and workpiece interface by using graphene nanofluid lubricant, *Int. J. Adv.*  
776 *Manuf. Technol.* 104 (2019) 3943–3958. doi:10.1007/s00170-019-04129-8.
- 777 [12] H. Singh, V.S. Sharma, S. Singh, M. Dogra, Nanofluids assisted environmental friendly  
778 lubricating strategies for the surface grinding of titanium alloy: Ti6Al4V-ELI, *J. Manuf. Process.*  
779 39 (2019) 241–249. doi:10.1016/j.jmapro.2019.02.004.
- 780 [13] G. Żyła, J. Fal, P. Estellé, Thermophysical and dielectric profiles of ethylene glycol based  
781 titanium nitride (TiN-EG) nanofluids with various size of particles, *Int. J. Heat Mass Transf.*  
782 113 (2017) 1189–1199. doi:10.1016/j.ijheatmasstransfer.2017.06.032.
- 783 [14] G. Żyła, J.P. Vallejo, J. Fal, L. Lugo, Nanodiamonds – Ethylene Glycol nanofluids:  
784 Experimental investigation of fundamental physical properties, *Int. J. Heat Mass Transf.* 121  
785 (2018) 1201–1213. doi:10.1016/j.ijheatmasstransfer.2018.01.073.
- 786 [15] G. Żyła, Nanofluids containing low fraction of carbon black nanoparticles in ethylene glycol:  
787 An experimental study on their rheological properties, *J. Mol. Liq.* 297 (2020) 111732.  
788 doi:10.1016/j.molliq.2019.111732.
- 789 [16] S. Zeinali Heris, M.A. Razbani, P. Estellé, O. Mahian, Rheological Behavior of Zinc-Oxide  
790 Nanolubricants, *J. Dispers. Sci. Technol.* (2015). doi:10.1080/01932691.2014.945595.
- 791 [17] N.A.C. Sidik, I.M. Adamu, M.M. Jamil, G.H.R. Kefayati, R. Mamat, G. Najafi, Recent progress  
792 on hybrid nanofluids in heat transfer applications: A comprehensive review, *Int. Commun. Heat*  
793 *Mass Transf.* 78 (2016) 68–79. doi:10.1016/j.icheatmasstransfer.2016.08.019.
- 794 [18] N.A. Che Sidik, M. Mahmud Jamil, W.M.A. Aziz Japar, I. Muhammad Adamu, A review on

- 795 preparation methods, stability and applications of hybrid nanofluids, *Renew. Sustain. Energy*  
796 *Rev.* 80 (2017) 1112–1122. doi:10.1016/j.rser.2017.05.221.
- 797 [19] M.H. Ahmadi, A. Mirlohi, M. Alhuyi Nazari, R. Ghasempour, A review of thermal conductivity  
798 of various nanofluids, *J. Mol. Liq.* 265 (2018) 181–188. doi:10.1016/j.molliq.2018.05.124.
- 799 [20] J.A. Ranga Babu, K.K. Kumar, S. Srinivasa Rao, State-of-art review on hybrid nanofluids,  
800 *Renew. Sustain. Energy Rev.* 77 (2017) 551–565. doi:10.1016/j.rser.2017.04.040.
- 801 [21] A. Asadi, I.M. Alarifi, L.K. Foong, An experimental study on characterization, stability and  
802 dynamic viscosity of CuO-TiO<sub>2</sub>/water hybrid nanofluid, *J. Mol. Liq.* 307 (2020) 112987.  
803 doi:10.1016/j.molliq.2020.112987.
- 804 [22] S.-R. Yan, R. Kalbasi, Q. Nguyen, A. Karimipour, Rheological behavior of hybrid MWCNTs-  
805 TiO<sub>2</sub>/EG nanofluid: A comprehensive modeling and experimental study, *J. Mol. Liq.* 308 (2020)  
806 113058. doi:10.1016/j.molliq.2020.113058.
- 807 [23] M. Afrand, K. Nazari Najafabadi, M. Akbari, Effects of temperature and solid volume fraction  
808 on viscosity of SiO<sub>2</sub>-MWCNTs/SAE40 hybrid nanofluid as a coolant and lubricant in heat  
809 engines, *Appl. Therm. Eng.* (2016). doi:10.1016/j.applthermaleng.2016.04.002.
- 810 [24] S.O. Giwa, M. Sharifpur, J.P. Meyer, S. Wongwises, O. Mahian, Experimental measurement of  
811 viscosity and electrical conductivity of water-based  $\gamma$ -Al<sub>2</sub>O<sub>3</sub>/MWCNT hybrid nanofluids with  
812 various particle mass ratios, *J. Therm. Anal. Calorim.* (2020). doi:10.1007/s10973-020-10041-  
813 1.
- 814 [25] Z. Tian, S. Rostami, R. Taherialekouhi, A. Karimipour, A. Moradikazerouni, H. Yarmand,  
815 N.W.B.M. Zulkifli, Prediction of rheological behavior of a new hybrid nanofluid consists of  
816 copper oxide and multi wall carbon nanotubes suspended in a mixture of water and ethylene  
817 glycol using curve-fitting on experimental data, *Phys. A Stat. Mech. Its Appl.* 549 (2020)  
818 124101. doi:10.1016/j.physa.2019.124101.
- 819 [26] I.M. Alarifi, A.B. Alkhouh, V. Ali, H.M. Nguyen, A. Asadi, On the rheological properties of  
820 MWCNT-TiO<sub>2</sub>/oil hybrid nanofluid: An experimental investigation on the effects of shear rate,  
821 temperature, and solid concentration of nanoparticles, *Powder Technol.* 355 (2019) 157–162.  
822 doi:10.1016/j.powtec.2019.07.039.
- 823 [27] S.U. Ilyas, R. Pendyala, M. Narahari, L. Susin, Stability, rheology and thermal analysis of  
824 functionalized alumina- thermal oil-based nanofluids for advanced cooling systems, *Energy*  
825 *Convers. Manag.* 142 (2017) 215–229. doi:10.1016/j.enconman.2017.01.079.
- 826 [28] G.M. Moldoveanu, A.A. Minea, M. Iacob, C. Ibanescu, M. Danu, Experimental study on  
827 viscosity of stabilized Al<sub>2</sub>O<sub>3</sub>, TiO<sub>2</sub> nanofluids and their hybrid, *Thermochim. Acta.* 659  
828 (2018) 203–212. doi:10.1016/j.tca.2017.12.008.
- 829 [29] S.U. Ilyas, M. Narahari, J.T.Y. Theng, R. Pendyala, Experimental evaluation of dispersion  
830 behavior, rheology and thermal analysis of functionalized zinc oxide-paraffin oil nanofluids, *J.*  
831 *Mol. Liq.* (2019). doi:10.1016/j.molliq.2019.111613.
- 832 [30] A. Banisharif, M. Aghajani, S. Van Vaerenbergh, P. Estellé, A. Rashidi, Thermophysical  
833 properties of water ethylene glycol (WEG) mixture-based Fe<sub>3</sub>O<sub>4</sub> nanofluids at low  
834 concentration and temperature, *J. Mol. Liq.* 302 (2020) 112606.  
835 doi:10.1016/j.molliq.2020.112606.
- 836 [31] M.H. Ahmadi, B. Mohseni-Gharyehsafa, M. Ghazvini, M. Goodarzi, R.D. Jilte, R. Kumar,  
837 Comparing various machine learning approaches in modeling the dynamic viscosity of  
838 CuO/water nanofluid, *J. Therm. Anal. Calorim.* 139 (2020) 2585–2599. doi:10.1007/s10973-  
839 019-08762-z.
- 840 [32] M. Ramezanizadeh, M.H. Ahmadi, M.A. Nazari, M. Sadeghzadeh, L. Chen, A review on the  
841 utilized machine learning approaches for modeling the dynamic viscosity of nanofluids, *Renew.*  
842 *Sustain. Energy Rev.* 114 (2019) 109345. doi:10.1016/j.rser.2019.109345.
- 843 [33] M. Vakili, S. Khosrojerdi, P. Aghajannezhad, M. Yahyaei, A hybrid artificial neural network-  
844 genetic algorithm modeling approach for viscosity estimation of graphene nanoplatelets  
845 nanofluid using experimental data, *Int. Commun. Heat Mass Transf.* 82 (2017) 40–48.  
846 doi:10.1016/j.icheatmasstransfer.2017.02.003.
- 847 [34] A.S. Dalkilic, A. Çebi, A. Celen, O. Yıldız, O. Acikgoz, C. Jumpholkul, M. Bayrak, K. Surana,  
848 S. Wongwises, Prediction of graphite nanofluids' dynamic viscosity by means of artificial neural  
849 networks, *Int. Commun. Heat Mass Transf.* 73 (2016) 33–42.

- 850 doi:10.1016/j.icheatmasstransfer.2016.02.010.
- 851 [35] M. Gholizadeh, M. Jamei, I. Ahmadianfar, R. Pourrajab, Prediction of nanofluids viscosity using  
852 random forest (RF) approach, *Chemom. Intell. Lab. Syst.* 201 (2020) 104010.  
853 doi:10.1016/j.chemolab.2020.104010.
- 854 [36] M.A. Marcos, L. Lugo, S. V. Ageev, N.E. Podolsky, D. Cabaleiro, V.N. Postnov, K.N. Semenov,  
855 Influence of molecular mass of PEG on rheological behaviour of MWCNT-based nanofluids for  
856 thermal energy storage, *J. Mol. Liq.* 318 (2020) 113965. doi:10.1016/j.molliq.2020.113965.
- 857 [37] F. Mashali, E.M. Languri, J. Davidson, D. Kerns, W. Johnson, K. Nawaz, G. Cunningham,  
858 Thermo-physical properties of diamond nanofluids: A review, *Int. J. Heat Mass Transf.* 129  
859 (2019) 1123–1135. doi:10.1016/J.IJHEATMASSTRANSFER.2018.10.033.
- 860 [38] R. Sadri, M. Hosseini, S.N. Kazi, S. Bagheri, N. Zubir, G. Ahmadi, M. Dahari, T. Zaharinie, A  
861 novel, eco-friendly technique for covalent functionalization of graphene nanoplatelets and the  
862 potential of their nanofluids for heat transfer applications, *Chem. Phys. Lett.* 675 (2017) 92–97.  
863 doi:10.1016/j.cplett.2017.02.077.
- 864 [39] J. Bin Wu, M.L. Lin, X. Cong, H.N. Liu, P.H. Tan, Raman spectroscopy of graphene-based  
865 materials and its applications in related devices, *Chem. Soc. Rev.* (2018).  
866 doi:10.1039/c6cs00915h.
- 867 [40] X. Li, L. Zhi, Graphene hybridization for energy storage applications, *Chem. Soc. Rev.* 47  
868 (2018) 3189–3216. doi:10.1039/c7cs00871f.
- 869 [41] S.U. Ilyas, S. Ridha, F.A. Abdul Kareem, Dispersion stability and surface tension of SDS-  
870 Stabilized saline nanofluids with graphene nanoplatelets, *Colloids Surfaces A Physicochem.*  
871 *Eng. Asp.* (2020). doi:10.1016/j.colsurfa.2020.124584.
- 872 [42] S. Chakraborty, P.K. Panigrahi, Stability of nanofluid: A review, *Appl. Therm. Eng.* 174 (2020)  
873 115259. doi:10.1016/j.applthermaleng.2020.115259.
- 874 [43] S.U. Ilyas, R. Pendyala, N. Marneni, Stability of Nanofluids, *Eng. Appl. Nanotechnol.* (2017)  
875 1–31. doi:10.1007/978-3-319-29761-3\_1.
- 876 [44] S.U. Ilyas, M. Narahari, R. Pendyala, Rheological characteristics of ultrastable diamond-thermal  
877 oil nanofluids, *J. Mol. Liq.* (2020). doi:10.1016/j.molliq.2020.113098.
- 878 [45] S.U. Ilyas, R. Pendyala, M. Narahari, Stability and thermal analysis of MWCNT-thermal oil-  
879 based nanofluids, *Colloids Surfaces A Physicochem. Eng. Asp.* 527 (2017) 11–22.  
880 doi:10.1016/j.colsurfa.2017.05.004.
- 881 [46] M.J. Rosen, J.T. Kunjappu, *Surfactants and Interfacial Phenomena*, John Wiley & Sons, Inc.,  
882 Hoboken, NJ, USA, 2012. doi:10.1002/9781118228920.
- 883 [47] S.M.S. Murshed, P. Estellé, A state of the art review on viscosity of nanofluids, *Renew. Sustain.*  
884 *Energy Rev.* 76 (2017) 1134–1152. doi:10.1016/j.rser.2017.03.113.
- 885 [48] A. Gallego, K. Cagua, B. Herrera, D. Cabaleiro, M.M. Piñeiro, L. Lugo, Experimental evaluation  
886 of the effect in the stability and thermophysical properties of water-Al<sub>2</sub>O<sub>3</sub> based nanofluids  
887 using SDBS as dispersant agent, *Adv. Powder Technol.* 31 (2020) 560–570.  
888 doi:10.1016/j.appt.2019.11.012.
- 889 [49] S. Zeroual, P. Estellé, D. Cabaleiro, B. Vigolo, M. Emo, W. Halim, S. Ouaskit, Ethylene glycol  
890 based silver nanoparticles synthesized by polyol process: Characterization and thermophysical  
891 profile, *J. Mol. Liq.* 310 (2020) 113229. doi:10.1016/j.molliq.2020.113229.
- 892 [50] J.P. Vallejo, G. Żyła, J. Fernández-Seara, L. Lugo, Rheological behaviour of functionalized  
893 graphene nanoplatelet nanofluids based on water and propylene glycol:water mixtures, *Int.*  
894 *Commun. Heat Mass Transf.* 99 (2018) 43–53. doi:10.1016/j.icheatmasstransfer.2018.10.001.
- 895 [51] J.P. Vallejo, S. Gómez-Barreiro, D. Cabaleiro, C. Gracia-Fernández, J. Fernández-Seara, L.  
896 Lugo, Flow behaviour of suspensions of functionalized graphene nanoplatelets in propylene  
897 glycol–water mixtures, *Int. Commun. Heat Mass Transf.* 91 (2018) 150–157.  
898 doi:10.1016/j.icheatmasstransfer.2017.12.001.
- 899 [52] J. Liebrecht, X. Si, B. Sauer, H. Schwarze, Investigation of drag and churning losses on tapered  
900 roller bearings, *Stroj. Vestnik/Journal Mech. Eng.* 61 (2015) 399–408. doi:10.5545/sv-  
901 *jme.2015.2490*.
- 902 [53] Swep, *Industrial handbook introduction - oil as a heat transfer fluid*, (n.d.).  
903 doi:<https://www.swep.net/industrial-handbook/industrial-handbook/>.
- 904 [54] Yukun Engineering Standards, *Data Sheets: Formulas/Nomograms (Part 4) Viscosity Vs.*

- 905 Temperature Charts, n.d.
- 906 [55] H. Nguyen-Schäfer, Applied tribology in the oil-film bearings, in: Springer Tracts Mech. Eng.,  
907 2015. doi:10.1007/978-3-319-17644-4\_9.
- 908 [56] Encyclopedia of Lubricants and Lubrication, 2014. doi:10.1007/978-3-642-22647-2.
- 909 [57] J.-B. Wu, M.-L. Lin, X. Cong, H.-N. Liu, P.-H. Tan, Raman spectroscopy of graphene-based  
910 materials and its applications in related devices, Chem. Soc. Rev. 47 (2018) 1822–1873.  
911 doi:10.1039/C6CS00915H.
- 912 [58] D. Cabaleiro, M.J. Pastoriza-Gallego, C. Gracia-Fernández, M.M. Piñeiro, L. Lugo, Rheological  
913 and volumetric properties of TiO<sub>2</sub>-ethylene glycol nanofluids, Nanoscale Res. Lett. 8 (2013)  
914 286. doi:10.1186/1556-276X-8-286.
- 915 [59] D. Gómez-Díaz, J.M. Navaza, Rheology of aqueous solutions of food additives: Effect of  
916 concentration, temperature and blending, J. Food Eng. 56 (2003) 387–392. doi:10.1016/S0260-  
917 8774(02)00211-X.
- 918 [60] G. Tammann, W. Hesse, Die Abhängigkeit der Viskosität von der Temperatur bei unterkühlten  
919 Flüssigkeiten, Zeitschrift Für Anorg. Und Allg. Chemie. 156 (1926) 245–257.  
920 doi:10.1002/zaac.19261560121.
- 921 [61] E.I. Cherecheş, J.I. Prado, C. Ibanescu, M. Danu, A.A. Minea, L. Lugo, Viscosity and isobaric  
922 specific heat capacity of alumina nanoparticle enhanced ionic liquids: An experimental  
923 approach, J. Mol. Liq. (2020). doi:10.1016/j.molliq.2020.114020.
- 924 [62] A. Karimipour, S. Ghasemi, M.H.K. Darvanjooghi, A. Abdollahi, A new correlation for  
925 estimating the thermal conductivity and dynamic viscosity of CuO/liquid paraffin nanofluid  
926 using neural network method, Int. Commun. Heat Mass Transf. 92 (2018) 90–99.  
927 doi:10.1016/j.icheatmasstransfer.2018.02.002.
- 928 [63] N. Zhao, Z. Li, Experiment and artificial neural network prediction of thermal conductivity and  
929 viscosity for alumina-water nanofluids, Materials (Basel). 10 (2017). doi:10.3390/ma10050552.
- 930 [64] A. Barati-Harooni, A. Najafi-Marghmaleki, A. Mohebbi, A.H. Mohammadi, On the estimation  
931 of viscosities of Newtonian nanofluids, J. Mol. Liq. 241 (2017) 1079–1090.  
932 doi:10.1016/j.molliq.2017.06.088.
- 933 [65] J.F.-A. of statistics, undefined 2001, Greedy function approximation: a gradient boosting  
934 machine, JSTOR. (n.d.).
- 935 [66] M. Si, K. Du, Development of a predictive emissions model using a gradient boosting machine  
936 learning method, Environ. Technol. Innov. 20 (2020) 101028. doi:10.1016/j.eti.2020.101028.
- 937 [67] J. Jiang, Y. Tzeng, Mechanisms of suppressing secondary nucleation for low-power and low-  
938 temperature microwave plasma self-bias-enhanced growth of diamond films in argon diluted  
939 methane, AIP Adv. 1 (2011) 042117. doi:10.1063/1.3656241.
- 940 [68] M. Muthuraj, J. Bensam Raj, J. Sunil, Experimental Investigation on the Influence of Graphene  
941 Nanoplatelets Dispersion on the Thermal Conductivity of Sunflower Oil, Int. J. Nanosci. 19  
942 (2020) 1950011. doi:10.1142/S0219581X1950011X.
- 943 [69] T.S. Krishnakumar, S.P. Viswanath, S.M. Varghese, J. Prakash M, Experimental studies on  
944 thermal and rheological properties of Al<sub>2</sub>O<sub>3</sub>-ethylene glycol nanofluid, Int. J. Refrig. 89 (2018)  
945 122–130. doi:10.1016/j.ijrefrig.2018.03.008.
- 946 [70] M. Afrand, D. Toghraie, B. Ruhani, Effects of temperature and nanoparticles concentration on  
947 rheological behavior of Fe<sub>3</sub>O<sub>4</sub>-Ag/EG hybrid nanofluid: An experimental study, Exp. Therm.  
948 Fluid Sci. 77 (2016) 38–44. doi:10.1016/j.expthermflusci.2016.04.007.
- 949 [71] S. Hamze, D. Cabaleiro, T. Maré, B. Vigolo, P. Estellé, Shear flow behavior and dynamic  
950 viscosity of few-layer graphene nanofluids based on propylene glycol-water mixture, J. Mol.  
951 Liq. 316 (2020) 113875. doi:10.1016/j.molliq.2020.113875.
- 952 [72] S.U. Ilyas, R. Pendyala, M. Narahari, Rheological behavior of mechanically stabilized and  
953 surfactant-free MWCNT-thermal oil-based nanofluids, Int. Commun. Heat Mass Transf. 87  
954 (2017). doi:10.1016/j.icheatmasstransfer.2017.07.015.
- 955